We are IntechOpen,
the world's leading publisher of
Open Access books
Built by scientists, for scientists

6,900
Open access books available

185,000
International authors and editors

200M
Downloads

154
Countries delivered to

Our authors are among the

TOP 1%
most cited scientists

12.2%
Contributors from top 500 universities

BOOK CITATION INDEX
CLARIVATE ANALYTICS
INDEXED

WEB OF SCIENCE™

Selection of our books indexed in the Book Citation Index
in Web of Science™ Core Collection (BKCI)

Interested in publishing with us?
Contact book.department@intechopen.com

Numbers displayed above are based on latest data collected.
For more information visit www.intechopen.com

Estimating Actual Evapotranspiration using ALARM and the Dimensionless Temperature

Ayman Suleiman and Jawad Al-Bakri
Land, Water and Environment Department, Faculty of Agriculture
University of Jordan, Amman,
Jordan

1. Introduction

Estimates of evapotranspiration, ET, are needed for many applications in diverse disciplines such as agriculture and hydrology. Many studies of long-term averages have shown that more than half of the net solar energy, and subsequently two thirds of precipitation, goes to ET (Brutsaert, 1982). ET is linked to the land surface energy budget as follows (e.g., Brutsaert, 1982):

$$R_n - G = H + E \tag{1}$$

where R_n (W m-2) is the net incoming radiation, G is the heat flux into the ground (W m-2), and H (W m-2) and E (W m-2) are the sensible and latent (evaporative) heat fluxes into the atmosphere. For the energy balance to close, any part of (R_n - G) that does not contribute to E must be converted into H. In order for that to happen, the surface has to have the temperature (T_s) that forces the energy balance to close. Estimation of H (or ET as a residual) over vegetated terrain is based on an aerodynamic temperature (T_i), which is the temperature that gives the correct value of H at a specified value (denoted $z_{0h,i}$) of the scalar roughness length, z_{0h}, based on Monin-Obukhov Similarity (MOS) theory in the surface sub-layer (Brutsaert, 1982; Stull, 1988). Specification of the value of z_{0h} to give the correct value of H for use with a radiometric surface temperature T_r is a difficult problem (e.g., Mahrt and Vickers, 2004); Crago and Suleiman (2005) outlined a method (discussed here in section 2.a) to specify $z_{0h,i}$ and to convert T_r to T_i. In the MOS theory, the flux is proportional to the difference between T_i and air temperature (T_a), with the ratio H / (T_i-T_a) depending on variables characterizing the atmospheric turbulence and the land surface. This relationship can be expressed as (e.g., Brutsaert, 1982):

$$H = \frac{(T_s - T_a)ku_*\rho c_p}{\left[\ln\left(\frac{z_a - d_0}{z_{0h}}\right) - \psi\left(\frac{z_a - d_0}{L}\right)\right]} \tag{2}$$

where T_s (C°) is the surface temperature, T_a (C°) is the air temperature at a height z_a (m) in the surface sublayer, *k* (where k=0.4) is von-Karman's constant, u_* (ms-1) is the friction velocity, ρ (kg m-3) is the density of the air, c_p (J kg-1 K-1) is the specific heat at constant

pressure, z_{0h} (m) is the scalar roughness length for sensible heat, and d_0 (m) is the displacement height. Atmospheric stability, which affects the efficiency of turbulent transport, is included by means of ψ, which is a function of the stability or buoyancy parameter $(z_a-d_0)/L$, where L (m) is the Obukhov length.

Once T_i is known it can be applied to calculate H (equation 2) and then actual ET can be obtained as a residual (equation 1). In one example, the accuracy of regional scale actual ET [obtained as a residual from (1) after finding H using (2), with T_a measured at a single point within the region] is approximately 70-80% (Wang et al., 2005). Models have been developed to improve accuracy through the use of radiometric surface temperature (Hatfield et al., 1983; Ben-Asher et al., 1992; Kustas et al., 2007; Anderson et al., 2007), leaf area index (LAI) (Consoli et al., 2005) and net radiation (Bandara, 2003) available from visible and infrared bands of satellite data. One example of ET modeling from remote sensing data is the Surface Energy Balance Algorithm for Land (SEBAL) which uses an empirical relationship between radiometric surface temperature and the difference between aerodynamic surface temperature and air temperature for each pixel (Bastiaanssen et al., 1998). Several studies (e.g. Menenti and Choudhury, 1993; Bastiaanssen and Chandrapala, 2003; Chandrapala and Wimalasuriya, 2003; Allen et al., 2005; Tasumi et al., 2005; Wang et al., 2005) used and modified SEBAL for spatial estimates of ET with remote sensing and weather data.

In order to implement SEBAL to estimate ET, it must be possible to identify a wet pixel and a dry pixel within an area of interest, and it must be reasonable to assume that atmospheric conditions aloft are horizontally uniform over that area. When one or both of these conditions cannot be met, the Surface Energy Balance Index (SEBI) can be used to calculate relative ET using a ratio of temperature differences (Roerrink and Menenti, 2000). The minimum surface temperature difference is obtained by solving the similarity equation for the minimum sensible heat flux that is found as a residual after determining the potential ET while the maximum surface temperature difference is determined by assuming that ET is zero. Since these bounds are pixel-dependant, potential ET has to be calculated for each pixel.

Suleiman and Crago (2004) developed a dimensionless temperature that does not require information from wet and dry pixels nor potential ET. For each pixel, the maximum surface temperature is determined by assuming that ET for the pixel is zero and the minimum temperature is determined by assuming that sensible heat flux is zero. This approach is advantageous in practice especially when a dry pixel is not available (Qiu et al., 2006). The dimensionless temperature Δ_T can be defined as $(T_i - T_a)/(T_{max} - T_a)$, where T_i is the aerodynamic surface temperature, T_a is the air temperature and T_{max} is the surface temperature that would occur if all the available energy ($R_n - G$) was converted to sensible heat flux (H) and no evaporation occurred. The dimensionless temperature procedure was used for mapping ET at a local scale with hydrological applications at riparian meadow restoration sites in California, USA (Loheide and Gorelick, 2005).

The Analytical Land Atmosphere Radiometer Model (ALARM) has been developed to convert the radiometric surface temperature T_r to the aerodynamic surface temperature T_i at any view angle (Crago, 1998; Suleiman and Crago, 2002a). ALARM converts radiometric surface temperature measured at any view angle to a well-defined aerodynamic surface temperature (T_i) by correcting for vegetation temperature profile and considering LAI, canopy height, fractional cover, leaf angle distribution, and sensor zenith view angle. ALARM worked well for varied canopy density when the zenith view angle was less than 20º and satisfactorily for view angles greater than 20º (Suleiman and Crago, 2002b; Zibognon et al., 2002). Other models such as Lhomme *et al.* (2000) and Massman (1999) also worked best at near-nadir view angles (Suleiman and Crago, 2002a).

2. Theoretical background

a. ALARM description

Within ALARM, the foliage is assumed to have an exponential vertical temperature profile (Brutsaert and Sugita, 1996) as follows:

$$T_f = T_{fg} + \left(T_{fh} - T_{fg}\right)e^{-b\zeta}, \tag{3}$$

where T_f is the temperature of the foliage at a height z above the soil surface, T_{fh} is the foliage temperature at the top of the canopy, T_{fg} is the asymptotic limit of the exponential foliage temperature profile, far below the bottom of the canopy, $\zeta = (h-z)/h$ is the dimensionless depth into the canopy, h is the canopy height, and b is a decay constant. Qualls and Yates (2001) observed an exponential vertical temperature profile within a grass canopy.

ALARM converts radiometric surface temperature measured at any view angle to a well-defined aerodynamic surface temperature (T_i) by correcting for vegetation temperature profile and considering LAI, canopy height, fractional cover, leaf angle distribution, and zenith sensor view angle as follows:

$$T_i = T_r + \left(T_{fg} - T_{fh}\right)(w - W). \tag{4}$$

where W is defined below in (7) and w can be derived (Crago, 1998) as:

$$w = \left(1 - f_{soil}e^{-b}\right)\left[\frac{\mu_r b}{g'LAI} + 1\right]^{-1} \tag{5}$$

In (5), $f_{soil} = \exp\left[-g'(LAI)/\mu_r\right]$ is the fraction of soil seen by the IRT (Friedl and Davis, 1994), μ_r is the cosine of the view zenith angle, and g' is taken as 0.5 which corresponds to a spherical leaf angle distribution and is representative of a wide range of vegetation types. When $T_{fh} = T_{fg}$, the canopy is isothermal. Under these conditions, Brutsaert and Sugita (1996) showed that the resulting scalar roughness length, $z_{0h,i}$, is given by:

$$z_{0h,i} = z_0 \exp\left[\frac{h}{(h-d_0)r_2} + \ln\left(\frac{h-d_0}{z_0}\right)\right]. \tag{6}$$

where d_0 is zero plane displacement height, z_o is momentum roughness length, and r_2 is defined below equation (7). The "aerodynamic" surface temperature T_i found with (4) is actually the "equivalent isothermal surface temperature" (Brutsaert and Sugita, 1996), or the value of T_s needed in (2) to estimate the correct H using the $z_{0h,i}$ for z_{0h}. Alternatively, T_i is the temperature the surface would require to give the correct sensible heat flux if the canopy was isothermal. The r_2 is given by $r_2 = [a - (a^2 + 4C_2)^{1/2}]/2$ and In (4), W is:

$$W = -(r_2 + b)C_2 / \left[r_2\left(b^2 + ba - C_2\right)\right], \tag{7}$$

In turn, $C_2 = 2(LAI)(Ct_f) h/[k (h-d_0)]$ and Ct_f is the transfer coefficient in the bulk transfer equation for the foliage elements, given by $Ct_f = C_L Re_*^{-m}Pr^{-n}$. The variable a is an exponential decay parameter of eddy diffusivity, Pr is the Prandtl number, and the Reynold's number

appropriate for transport through a leaf boundary layer is $Re_* = u_* L_f / v$, where L_f is the characteristic length scale of a leaf and v is the kinematic viscosity.

In (5), w is a weighting coefficient, describing the importance of T_{fh} and T_{fg} in determining the radiometric surface temperature seen by a radiometer:

$$T_r = w T_{fh} + (1 - w) T_{fg} \tag{8}$$

Similarly, W is a weighting coefficient describing the relative importance of T_{fh} and T_{fg} in producing sensible heat flux.

b.   ALARM parameterization

The ALARM model has several variables (T_{fh}, b, a, and d_0/h) that need to be parameterized, all of which have real physical meanings independent of the means of measuring surface temperature. Crago and Suleiman (2005), on a study at different sites with varying LAI, found that the use of a generalized parameterization for these variables at the different sites gave sensible heat flux values comparable to those obtained using localized parameterization. Based on their findings, they recommended the following generalized parameterization for the four variables ((T_{fh}, b, a, and d_0/h):

$$T_{fh} = T_a \tag{9}$$

where T_a is the air temperature at the top of the canopy.

The parameter b controls the rate at which foliage temperature increases with depth into the canopy and was parameterized as a function of LAI:

$$b \quad = \quad 0.75 \quad for LAI \geq 1.87, \tag{10}$$

and

$$b \quad = \quad 3.7 - 1.58 LAI \quad for LAI < 1.87. \tag{11}$$

Previous work with ALARM (Zibognon et al, 2002; Suleiman and Crago, 2002a and b) suggests that the parameters a and d_0/h can influence the estimates of ET. Specifically, larger values of a (near 5) effectively confine turbulence and turbulent transport to the top layers of the model canopy, while smaller values (near 0) allow turbulence. They were parameterized as follows:

$$a \quad = \quad 0.5 LAI, \tag{12}$$

and

$$d_0 / h = 0.335 a \tag{13}$$

c.   Dimensionless temperature

Suleiman and Crago (2004) introduced a dimensionless temperature (Δ_T) as follows:

$$\Delta_T = \left(\frac{T_i - T_a}{T_{max} - T_a} \right) \tag{14}$$

A value of T_{max} can be obtained by solving for T_s in Eq. [2], assuming that H equals (R_n - G). Also T_{max} may be assumed equals to the surface temperature of a hot pixel for heterogonous surfaces. Such an assumption would reduce the number of weather data needed.

The relationship between H and Δ_T is approximately linear, and goes through the origin [assuming the denominator of (2) varies little as T_s goes from T_i to T_{max}]:

$$H = (R_n - G)\Delta_T \qquad (15)$$

The relationship between E and Δ_T is:

$$E = (R_n - G)(1 - \Delta_T) \qquad (16)$$

and the evaporative fraction EF is:

$$EF = \frac{E}{(R_n - G)} = 1 - \Delta_T = \frac{T_{max} - T_i}{T_{max} - T_a} \qquad (17)$$

The dimensionless temperature Δ_T can be found from (14) using ALARM T_i, measured T_a, and T_{max} found as described above. Scaling T_i using the dimensionless procedure reduces the sensitivity of ET estimates to errors in T_a and T_r. The assumption of a constant evaporative fraction, EF = E / R_n, was implemented to extend instantaneous to daily ET because orbiting satellites usually provide coverage only once a day.

In all, there are three major assumptions in the integrated ALARM and dimensionless algorithms. Within ALARM, the foliage is assumed to have an exponential vertical temperature profile. Such an assumption should be generally valid during the satellite pass in the middle of the day because exponential foliage vertical temperature profiles are more evident in the middle of the day. The relationship between H and Δ_T is assumed to be linear, and goes through the origin. This assumption should not result in any serious errors in the estimation of ET especially that the variation of the dominator of (2) is little as T_s goes from T_i to T_{max}. The assumption of a constant evaporative fraction contributes to uncertainty in ET estimates but these uncertainties should be most of the time minimum in semiarid climatic conditions. The implementation of the constant evaporative fraction assumption usually yields accurate daily ET estimates for cloud-free days, as indicated by Zhang and Lemeur (1995). However, variations in cloudiness during the day may produce some uncertainties in ET estimates because clouds at times other than the time when the satellite passes may invalidate the constant-EF assumption. This effect, i.e., varying EF during mid day hours has been found from numerous observations to vary little (e.g., Shuttleworth *et al.*, 1989; Gurney and Hsu, 1990, Brutsaert and Chen, 1996; Crago and Brutsaert, 1996; Lhomme and Elguero, 1999) and it has been found that it depends on the site and time of year (Kustas et al., 1993). In semiarid areas under a wide range of conditions, Kustas et al. (1993) found that the correlation coefficient between midday and daytime EF was rather high (r = 0.92).

Figure1 shows the inputs and steps of actual hourly and daily ET calculations suing ALARM and the dimensionless temperature (ALARMD).

d. FAO-56 and ASCE evapotranspiration

Daily actual ET was obtained from the FAO-56 grass reference ET (ET_o) approach in order to compare it with the ALARM actual ET. Allen et al. (1998; 2005) emphasized that the FAO-56 Penman-Monteith (PM) reference ET (ET_o) would provide reasonable estimates of ET under various climatic conditions. The FAO-56 ET_o was developed for a hypothetical well-watered and actively growing uniform grass of 0.12 m height with a surface resistance of 70 s m^{-1} and an albedo of 0.23 (Allen et al., 1998). The equation for a grass reference crop according to Allen et al. (1998) is defined as follows:

$$ET_o\left(\text{mm d}^{-1}\right) = \frac{0.408\Delta(R_n - G) + \gamma\dfrac{900}{T + 273}u_2\left(e_s - e_a\right)}{\Delta + \gamma\left(1 + 0.34u_2\right)} \tag{18}$$

where R_n is the net radiation (MJ m^2 d^{-1}), G the soil heat flux (MJ m^2 d^{-1}), T the mean daily air temp (°C), u_2 the mean daily wind speed at 2 m height (m s^{-1}), e_s-e_a the saturation vapor pressure deficit (kPa), Δ the slope of the vapor pressure-temperature curve (kPa °C^{-1}), and γ the psychometric constant (kPa °C^{-1}). The terms in the numerator on the right hand of the equation are available energy forcing and air dryness forcing, respectively (Kim and Entekhabi, 1997). Actual ET, ET_a is found from ET_0 as $ET_a = (K_s)(K_c)ET_0$, where K_c is the crop coefficient and K_s is a water stress coefficient (Allen et al., 1998). American Society of Civil Engineers (ACSE) (2005) alfalfa equation is similar to the FAO-56 with different resistance value.

3. Case studies

3.1 Jordan
3.1.1 Validation study

3.1.1.1 Data and methods

A validation study was undertaken using data from the Agricultural Research Station of the University of Jordan (ARSUJ) in the central Jordan Valley at 32° 10' N latitude and 35° 37'E longitude at an altitude of -230 m (below mean sea level). The station has a warm climate in winter with a minimum temperature of 8.5 °C in January and a hot summer with a maximum temperature of 40.4 °C in July. The yearly average maximum and minimum temperatures are 30.9 and 18.5 °C, respectively, while the yearly mean temperature is 24.7 °C. The experiment site was selected in an alfalfa field where an automated weather station (Campbell Scientific, Logan, UT) was installed. The crop wass irrigated with a sprinkler irrigation system twice to three times a week and planted on a sandy loam soil with good internal drainage. Data collected by the weather station included hourly and daily net solar radiation measured by a NR-LITE-L net radiometer (Kipp & Zonen USA Inc., Bohemia, NY), hourly and daily wind speed at 2 m measured using a R.M. Young wind sentry 03101-5 system (Campbell Scientific, Logan, UT), and air temperature and humidity measured at a height of 2 m using a shielded and aspirated REBS THP. ALARM used MODIS LAI, albedo and T_r along with hourly solar radiation, air temperature, and wind speed and daily and solar radiation.

The soil water content was monitored with TRIME tube access probe (P3, IMKO Micromodultechnik GmbH, Ettlingen, Germany). Five access tubes of 1 m height were installed in the field. The measurements of the volumetric soil water content with the TRIME probe at depths of 0-20, 20-40, 40-60, and 60-80 cm were conducted manually once a day in the morning from March to October 2006. A water balance equation was used to calculate the measured ET using the soil moisture readings as:

$$ET_m = I - D - \Delta W \tag{19}$$

Where ET_m is measured ET (mm d^{-1}), I is irrigation (mm d^{-1}), D is vertical drainage (mm d^{-1}), and ΔW is the change in soil water (mm d^{-1}). Only ET_m for days of no irrigation (I = 0) and zero D (D= 0) were used in this study to minimize the errors of ET_m. Because of the limited

number of usable satellite overpasses needed for use with ALARM, a total of twelve days of data were available for the validation study.

3.1.1.2 Results

Results from the validation study in the ARSUJ alfalfa field are shown in Figures 2, 3, and 4. Since the field was irrigated, ET rates ranged from about 6 to about 10 mm day^{-1}. For this range the Root Mean Square Error (RMSE) for ALARM (as compared to the TRIME probe reference values-referred to as "measured" values hereafter) was 0.87 mm day^{-1}, and coefficient of determination (r^2) was 0.36 while the RMSE for ASCE (2005) was 1.25 mm d^{-1} and r^2=0.06.

Errors in the ASCE (2005) and FAO-56 methods for moisture-stressed sites are likely to be dominated by errors in the water stress coefficient. Such errors are likely to be quite large when taken as a percent error of the daily ET, but relatively small in actual magnitude during very dry conditions. Assuming independent random errors equal to 1.25 mm day^{-1} in successive measurements, two daily FAO-56 measurements that differ by less than $(1.25^2+1.25^2)^{1/2}$ mm day^{-1} = 1.76 mm day^{-1} are not far enough apart to rule out random variability. Error magnitudes in the ALARM model are unlikely to vary greatly with the magnitude of the ET rate. Theoretically, EF varies with Δ_T, which is a ratio of two temperature differences . Absolute errors in both T_i and T_{max} are likely to be largest under conditions of high available energy, but under these conditions (T_i-T_a) and ($T_{max}-T_a$) are likely to be large, so the relative errors are likely to be similar for a wide range of conditions. Experimentally, Suleiman and Crago (2004) applied the dimensionless temperature approach (without the ALARM model) to grasslands under stressed and unstressed conditions, and found similar scatter of estimated to measured ET under high (up to about 5.5 mm day^{-1}) and low (down to about 1.5 mm day^{-2}) daily ET rates. Thus, assuming random and independent errors, it seems reasonable to assume that two daily ALARM measurements of ET that differ by less than $(0.87^2+0.87^2)^{1/2}$ mm day^{-1} = 1.2 mm day^{-1} are not far enough apart to rule out random variability. Finally, if ET_{aa} and ET_{fa} estimates are different by less than $(1.25^2+0.87^2)^{1/2}$ mm day^{-1}= 1.5 mm day^{-1}, they are not far enough apart to rule out random variability.

3.1.2 Comparison study

3.1.2.1 Data and methods

Six weather stations distributed within the different ecological zones in Jordan (Figure 5) were used in this study. The Rwaished site was located within the Saharo-Arabian region. The Safawi and Mafraq sites were located in the Irano-Turanian region. The Aqaba site was located within the Sudanian Penetration while the Irbed and Amman sites were located within the Mediterranean region. Monthly precipitation for the study sites is shown in Table 1. The high variation of monthly and total rainfall amounts from one site to another is apparent in Table 1.

Land use/cover of each site was derived from visual interpretation of high resolution Landsat ETM+ (Enhanced Thematic Mapper plus) images using an onscreen digitizing procedure for each of the 1 × 1 km pixels containing the study sites. Output from land use/cover mapping of each site was used to calculate the weighted average of water stress and crop coefficients (K_sK_c), shown in Table 2, which was required to convert ET_o to actual ET.

Eight-day 1-km leaf area index (LAI), albedo and instantaneous 4-km radiometric surface temperature (T_r) were obtained from the Moderate Resolution Imaging Spectroradiometer (MODIS) Terra instrument for April 2002 for the six sites. Linear interpolation was used to obtain daily LAI from the 8-day LAI. Although a functional relationship between LAI and plant canopy height (h) is vegetation dependent, h was estimated from LAI as h (m) = 0. 2 LAI when LAI was greater than or equal to 0.5 and h (m) = 0.1 when LAI was less than 0.5. The range of LAI and T_r and the number of days for which T_r was available in April for the different sites are shown in Table 3. The LAI was less than 0.5 for Rwaished, Safawi and Aqaba and more than 0.7 for Mafraq, Irbed and Amman. The MODIS T_r was lowest in Irbed and Amman and greatest in Rwaished and Safawi. The number of days for which MODIS T_r was available in April 2002 varied from one site to another. It ranged from 23 occurrences (77 %) at Aqaba to 13 in Mafraq (43 %).

The 2001/2002-season was wet, with few cold days (minimum air temperature of 4.8 C^o at Mafraq) and some hot days (maximum air temperature of 34.5 C^o at Aqaba and Rwaished) towards the end of April. According to the official climatic records (JMD, 2002; http://www.jmd.gov.jo), the 2001/2002 rainfall season was above average for all sites, except Aqaba. Irbed had the highest precipitation amounts in April, then Amman Airport, and then Mafraq while the other three stations received 0 or about 0 rainfall (Table 1). Wind speed (u) was measured at a height of 2 m four times a day at 12 am, 6 am, 12 pm and 6 pm local time. The *u* at 12 pm (noon) was used in this study since it was the closest to the time of Terra MODIS passes (10 am to 12 pm) over the six sites.

Hourly and daily solar radiation and air temperature at 2 m height were obtained from SoDa ((Solar Data) server (http://www.soda-is.com/eng/index.html) (Wald et al., 2002). The downward solar radiation data were found from the NCEP/NCAR daily values reanalysis. The server makes online query to the archive (1958-onwards) of NCEP/NCAR database for radiation parameters, air temperature and precipitation (National Centers for Environmental Prediction / National Center for Atmospheric research, USA). The server is mirrored by Institute Pierre-Simon Laplace, France. The hourly and daily net longwave irradiance was calculated using Allen et al. (1998) procedure. The heat flux into the ground (G) varies during the day and it depends on many factors such as leaf area index and soil moisture. However, it is strongly correlated with net radiation and it is often assumed to be 30% of the net radiation (e.g., Santanello and Friedl, 2003). Hence, in this study for simplicity the same assumption was employed. In open range areas, K_s was assumed to be 0.5 to account for the low soil moisture availability that resulted from limited rainfall amounts at the sites that have open range areas. For all other vegetation types, K_s was set equal to 1.0 throughout the study because green urban and irrigated olives areas were irrigated and because it was a wet year in Irbed. Following the recommendations and using the equations of Allen et al. (1998), the vapor pressure needed for ET_0 (equation 18) was found by assuming the dew point temperature for each day was equal to the minimum temperature for that day.

3.1.2.2 Results

Air and MODIS radiometric surface temperatures in April 2002 for the different sites are shown in Figure 6. The two highest radiometric surface temperatures and the highest differences between radiometric surface and air temperatures were seen in Rwaished and Safawi. The difference between radiometric surface and air temperature was lowest in Irbed where in some instances it was negative. Dimensionless temperature (Δ_T) was greater than 0

for all the days for all the locations except Irbed, which had 6 instances of negative Δ_T, two of which were < -0.50 (Figure 7). The influence of warm advection at Irbed will be discussed later. The positive Δ_T values ranged from 0.09 for Irbed to about 0.80 for Rwaished and Safawi.

The maximum ALARM actual ET, ET_{aa} ranged from 2.4 mm d^{-1} in Safawi to 6.5 mm d^{-1} in Irbed while the maximum FAO-56 actual ET, ET_{fa} ranged from 1.7 mm d^{-1} in Mafraq to 7.1 mm d^{-1} in Irbed (Table 4). The minimum ET_{aa} ranged from 0.7 mm d^{-1} in Safawi to 1.5 mm d^{-1} in Mafraq while the minimum ET_{fa} ranged from 0.7 mm d^{-1} in Aqaba to 3.7 mm d^{-1} in Irbed. The average of ET_{aa} and ET_{fa} were almost identical in Amman, within 0.7 mm d^{-1} in Rwaished, Safawi, Mafraq, and Aqaba and greater than 1 mm d^{-1} in Irbed (Table 4). These results indicate that generally there is a good agreement between minimum, maximum, and average ET_{aa} and ET_{fa} at all sites but Irbed for which the minimum and consequently the average ET_{aa} and ET_{fa} were different.

At three of the sites (Rwaished, Safawi and Amman), ET_{aa} and ET_{fa} were similar throughout April (Figure 8). At the Amman site, ET_{aa} appeared to fluctuate from one day to another throughout April. However, ET_{aa} and ET_{fa} from DOY 95- 104 both fluctuated over a wider range than they did from DOY 108- 120. In the case of ET_{fa}, the fluctuations were smaller than 1.76 mm day^{-1}, so random variations cannot be ruled out. The ET_{aa} fluctuations were on the order of 2 mm day^{-1}, which suggested they cannot be explained by random variations. One possible explanation is that soil moisture was reduced after DOY 104 and was unable to supply sufficient water to allow for high ET after this date. The drop in ET_{aa} near DOY 105 at Aqaba, which was also greater than 1.2 mm day-1, might have a similar explanation.

In Mafraq and Aqaba , ET_{aa} and ET_{fa} were close on most days. However, on some days there were larger differences. ET_{aa} was consistently a little higher than ET_{fa} in Mafraq and on most days in Aqaba. In Irbed, ET_{aa} and ET_{fa} were close on many days while ET_{aa} was lower than ET_{fa} on several days indicating that water stress may have taken place on these days. Due to its use of radiometric surface temperatures ET_{aa} is expected to respond automatically to water stress, while ET_{fa} can only respond by changing K_s. On the other hand, on four days ET_{aa} was greater than ET_{fa} indicating that warm advection was present. For five days, ET_{fa} was greater than 6 mm d^{-1} and for day 111 ET_{aa} was more than the reference ET (ET_o).

The ET_{aa} and ET_{fa} were much lower than ET_o for all the sites but Irbed. Generally, a good agreement was observed in the arid and semiarid sites which were utilized as open rangeland and in Amman where the irrigated area was 21%. On the other hand, little agreement was observed in Mafraq where 70% of the vegetation was denser due to the large fraction of protected rangeland and in Irbed where 75% of the site was cultivated, mainly with field crops (Table 2). For the sites of Safawi and Amman, the agreement between ET_{aa} and ET_{fa} was obvious and both curves nearly coincided after the day 105 (Figure 8). A similar trend with less agreement was observed in Rwaished and Aqaba.

In general, ET_{aa} had a well-defined linear relationship with Δ_T with some fluctuations due to the availability of energy (R_n-G) for ET (Figure 9). This relationship, which is mathematically described in equation (16), demonstrated that the dimensionless temperature and R_n-G are responsible for actual ET determination. Although R_n-G is the main factor that influences potential ET, Δ_T is a measure of the actual ET. Many points from the Irbed site deviated from the line because of the sensible heat advection, which resulted in higher actual ET_{aa} at very low (even negative) Δ_T.

Ideally, Δ_T ranges from 0 when ET is maximum (ET=R_n-G) to 1 when ET is minimum (ET=0). However, negative Δ_T can be found when warm advection takes place and the air temperature becomes higher than the aerodynamic surface temperature. The warm air in this case acts as another source of energy through downward (negative) sensible heat flux. A low value of Δ_T may suggest that a soil has sufficient moisture available to meet ET demands while a high value of Δ_T would indicate limited soil moisture availability. That is why Irbed, which received a relatively high rainfall amount, had the lowest Δ_T values and Rwaished and Safawi, which did not receive much rain, had the highest Δ_T values (Table 4). Continuous increase of Δ_T is a clear signal of decreasing water availability and increasing water stress. This coincided with the trend of herbaceous vegetation growth in Mafraq, where the green flush continued for a short period and quickly reduced the available soil moisture. Under such conditions, both soil water and vegetation type and density would likely affect the estimate of actual ET_{fa} from the FAO-56 equation (through the coefficients K_s and K_c, respectively). This was most clearly seen in Irbed and Mafraq where ET estimates from ALARM and FAO-56 were closest in periods following rainfall (Figure 7). Actual ET from both estimates was in relatively good agreement for the other sites that were less vegetated and were either urbanized or grazed rangelands.

Fluctuations of Δ_T from one day to another could also be due to the variability of the net solar radiation from one day to another. This was an expected behavior in all sites as the 1 km spatial resolution included a mixture of land use/covers. The presence of large increase and then decrease in Δ_T during drying periods (e.g., Mafraq around day 103) could be due to either a non-recorded small rain event that increased Δ_T in one day and then in the next Δ_T came back to where it was or that the high Δ_T was an outlier for some reasons. Nevertheless, a Δ_T value of about 0.35 to 0.40 suggests that potential ET was taking place while a Δ_T value of about 0.75 to 0.80 implies that soil evaporation is not contributing significantly to ET because of a dry soil surface and transpiration is not meeting the evaporative demand. Any Δ_T that is significantly less than about 0.30 is likely due to sensible heat advection because when Δ_T is about 0.30, ET seems to be close to potential ET.

The decreasing trends of actual ET may reflect drydown cycles of soil moisture due to ET and deep percolation. The contribution of deep percolation to the loss of soil water cannot be assessed without monitoring or simulating the change of the soil moisture profile due to drainage (Suleiman, 2008). The values of actual ET_{aa} and its range seemed reasonable although no site-specific calibration has been done. The trend of increasing ET_{aa} from DOY 100 to 104 in Aqaba could be attributed to the increase of air temperature during this period and the irrigation activities to the south of the site. The decrease of ET after that period was attributed to loss of soil water from the surrounding areas.

Because of the warm advection and the high wetness conditions the maximum and average actual ET were higher in Irbed than all the other sites (Table 4). The advection in Irbed is a well-known phenomenon that usually results in crop failure, particularly for lentil crops (NCARE, 2002a). Comparing the daily air temperature records (NCARE, 2002b) with the long-term averages (JMD, 2002) showed that the maximum air temperature was 7 C° above the average during this period. During the periods of advection the maximum air temperatures ranged from 29 to 31 C°, compared with an average value of less than 21°C. These results concurred with Rosenberg and Verma (1978) who found, in a study on irrigated alfalfa, that ET was greater than 10 mm d^{-1} on one-third of the days of studies. They attributed these high ET values to the contribution of sensible heat advection to ET. In

this study, the effect of advection on ET estimates was observed by ALARM and MODIS data while potential ET equations such as Priestley-Taylor are not capable of predicting such effects because they are developed for minimally-advective conditions (e.g., Brutsaert, 1982). The interaction of soil water and climatic factors resulted in high ET values in Irbed. Suleiman and Ritchie (2003) demonstrated that soil evaporation could be more than 10 mm d^{-1} when the saturated soil layers are close to the surface. This was possible in Irbed as the area had heavy clayey soils (MoA, 1994) known as vertisols. These soils are well known for their high water holding capacity. Therefore, higher values of ET were obtained for this site, as water from heavy rainfall was stored in the soil. However, the other sites were characterized by arid soils that received low rainfall amounts and subsequently lower ET values were noticed at these sites. Therefore, the impact of soil water availability and advection on the estimation of actual ET would suggest that ALARM might be able to provide a more accurate estimate of ET than the FAO-56 approach which assumed no water stress (Allen et al., 1998)

3.1.3 California case

3.1.3.1 Data and methods

Atmospherically corrected 1-km leaf area index (MOD11A1), 8-day albedo (MCD43B3),and instantaneous radiometric surface temperature (T_r) ((MOD15A2), were obtained from the Moderate Resolution Imaging Spectroradiometer(MODIS) and atmospherically corrected 90-m T_r (AST08) and 15-m surface reflectance product (AST07) for July 5th, 2008. These images were for a fully-irrigated alfalfa field located in Blythe, California (33° 28' 8"N latitude and 114° 42' 25"W longitude). Hourly wind speed was obtained from a nearby automated weather station.

The observed ET_c was determined from the surface renewal meteorological method (Snyder et al., 1996). The surface renewal system consisted of a Q7.1 net radiometer, two soil heat flux plates (Radiation and Energy Balance Systems, Inc.), and one set of spatially averaging soil temperature probes to measure net radiation, soil heat flux and soil heat storage, respectively. Two fine wire thermocouples (0.076 mm diameter) (Campbell Scientific, Inc.) mounted 1.5 m above the ground surface to measure air temperature fluctuations. The sensors were connected to CR10X data logger (Campbell Scientific, Inc.). Data processing procedures to determine the sensible heat flux density can be found in Snyder et al. (1996). The latent heat flux was then determined from the energy balance equation. The latent heat flux was lower but close to the net radiation from 8:00 am to 2:00 pm after which and until the end of the day, the latent heat flux was somewhat higher than the net radiation due to advection of heat. The sensible heat flux was negative (downward) throughout the day while the ground heat flux was negative (upward) at nighttime and positive at daytime.

To obtain ALARM-D and SEBAL hourly and daily ET_c, the surface renewal net radiation and ground heat flux were used. For SEBAL, The wet and dry pixels were assigned to the lowest and highest radiometric surface temperatures pixels, respectively. The sensible heat flux was assumed 0 for the wet pixel and the latent heat flux was assumed 0 for the dry pixel. The assumption of a constant evaporative fraction, EF = E / R_n, was implemented to extend instantaneous to daily ET_c because orbiting satellites, i.e., Terra-MODIS provides a coverage once in the daytime which was about 11:30 am on July 5th, 2008. The evaporative fraction has been found from numerous observations to vary little during the daytime (Crago and Brutsaert, 1996). The EF on July 5th, 2008 was fairly

constant at about 1.08 from 7:00 am in the morning to 2:00 pm after which it increased to about 1.35 by 7:00 pm (Figure 10).

3.1.3.2 Results

For the four ASTER 90-m pixels that have somewhat uniform vegetation, ALARM-D overestimated hourly ET_c in three pixels by 0.06 to 0.13 mm hr^{-1} and underestimated in one pixel, the pixel with maximum radiometric surface temperature, by 0.01 mm hr^{-1} while SEBAL underestimated hourly ET_c for all the pixels by 0.07 to 0.12 mm hr^{-1} (Table 5). On average ALARM-D overestimated hourly ET_c by 0.07 mm hr^{-1} whereas SEBAL underestimated hourly ET_c by 0.09 mm hr^{-1}. The relative error of hourly ET_c ranged from -1.1 to 14.9% for ALARM-D and -8 to -13.8% for SEBAL. Pixels that had relatively low absolute relative error for ALARM-D had relatively high absolute relative error for SEBAL and vice versa. Except for one pixel, the range of absolute relative error was comparable for ALARM-D and SEBAL.

For the ASTER 90-m pixels, ALARM-D overestimated daily ET_c in two pixels by 0.06 mm day^{-1} and underestimated in two pixels by 0.01 to 0.7 mm day^{-1} while SEBAL underestimated daily ET_c for all the pixels by 1.2 to 1.7 mm day^{-1} (Table 6). On average ALARM-D overestimated daily ET_c by 0.1 mm day^{-1} whereas SEBAL underestimated daily ET_c by 1.4 mm day^{-1}. The relative error of daily ET_c ranged from -8.1 to 7% for ALARM-D and -14 to –19.8% for SEBAL. The absolute relative error for ALARM-D was less than half of that for SEBAL for all the pixels. Having evaporative fraction higher towards the end of the day (after 2:00 pm) than the fairly constant evaporative fraction during the other hours (Figure 11) was the main reason why the ALARM-D daily ET_c overestimation was less than for the hourly ET_c.

For 1-km pixels at which the alfalfa field is spread, the difference between MODIS ALARM-D and SEBAL daily ET_c ranged from 0.2 to 1.2 mm day^{-1} (Table 7) while the difference between upscaled ASTER ALARM-D and SEBAL daily ET_c ranged from 0.7 to 2 mm day^{-1} (Table 8). That demonstrated that ALARM-D daily ET_c was higher than SEBAL daily ET_c for all the 1-km pixels. ASTER ALARM-D and SEBAL daily ET_c was greater than MODIS ALARM-D and SEBAL daily ET_c and closer to the surface renewal daily ET_c. Discrepancies between 1-km pixel and surface renewal daily ET_c are expected because of the variability in crop parameters such as leaf area index, soil moisture availability and microclimate.

4. Application of ALARM to monitor drought

4.1 Drought monitoring with earth observations

Drought is an extended period of deficiency in water supply results in a region due to insufficient precipitation, high evapotranspiration and overexploitation of water resources. Drought has adverse effects on the socioeconomic, agricultural, and environmental conditions. Jordan, located between 29° 11' N and 33° 22' N latitudes, and between 34° 19' E and 39 ° 18' E longitudes in the eastern Mediterranean region, is among the world's ten most water-limited countries. Most of the country's land is arid with low rainfall and high potential evaporation (Figure 12). The occurrence of drought in the country is highly variable through time and space depending on the actual rainfall, which falls between December and March, with high variability in intensity and duration of the individual showers. The agricultural sector, which represents a source of income for more than 15 percent of the population, continues to grapple with challenges of scarce water and the

frequent droughts. Therefore, monitoring of drought is one of the top priorities for rainfed agriculture.

Different methods of drought monitoring have been developed worldwide. The methods are based on drought-causative and drought-responsive parameters such as rainfall, soil moisture, potential evapotranspiration, and vegetation condition. The interest in the use of remote sensing data of different earth observation systems (EOS) started to increase in the last two decades. This could be attributed to the recent developments in these contemporary sources of information and to their availability in near real time. The use of remote sensing was also enhanced by the improved spatial and temporal resolutions, which could not be provided by the meteorological data. Among the most important sources of EOS data were those of MODIS land data (http://modis.gsfc.nasa.gov/), which could be downloaded from the web (https://wist.echo.nasa.gov/api/), free of charge. The free products of MODIS encouraged researchers and scientists to use the data for monitoring land resources of soil, vegetation and water. Recently, NASA launched the Land Atmosphere Near-Real-Time Capability for EOS (LANCE), which was designed to provide EOS data products within 3 hours of acquisition. The system was developed for near real-time applications and would be particularly relevant for agricultural monitoring. Access to LANCE data can be obtained at http://lance.nasa.gov/.

One of the most important products from EOS was the normalized difference vegetation index (NDVI), which was provided by the advanced very high resolution radiometer (AVHRR) in the 1980's and 1990's, followed by SPOT vegetation instrument in the 1990's and finally by MODIS in year 2000 and afterward. Two previous studies in Jordan (Al-Bakri and Taylor, 2003; Al-Bakri and Suleiman, 2004) showed that NDVI images were useful in tracing vegetation response to cumulative rainfall. Therefore, a drought monitoring unit at the National Center for Agricultural Research and Extension (NCARE) started to use MODIS-NDVI images for monitoring drought (Al-Naber et al., 2009). The implementation of NDVI images to monitor drought was based on comparing composite images of NDVI with the average of the time series for the particular period. This approach, however, was based on the assumption of normal distribution of NDVI which reduced the reliability of the outputs (Al-Naber et al., 2009). Alternatively, ALARMD was used to derive actual ET from MODIS and to calculate the Evapotranspiration Water Stress Index (EWSI) and to produce GIS maps that could be used to assess the severity of drought in Jordan. The EWSI was calculated as following:

$$EWSI = 1 - \left(\frac{ETa}{ETc} \right)$$ (20)

Where EWSI is evapotranpiration water stress indicator and ranges from 0 to 1 and ETa and ETc are daily actual and crop evapotranspiration.

4.2 Case study in Yarmouk basin in Jordan

The study area covers approximately 1400 km² and is characterized by an obvious rainfall gradient (Figure 12). The western parts of area are mainly rainfed where olive trees and wheat are planted, in addition to other crops of fruit trees and summer crops of vegetables. The eastern parts are extending in the low rainfall zone of the country where open grazing is practiced and rainfed barley is cultivated to support the grazing herds. Irrigation is taking place in different parts of the area using groundwater. The study area is extremely

important to Jordan in that it is the main source of surface water at the present time that discharges through the Yarmouk River. Also, it forms an important part of the rainfed area in the north of Jordan.

For the computation of Evapotranpiration Water Stress Indicator (EWSI) the actual daily evapotranspiration (ETa) was determined using ALARMD model. Some input data for ALARMD were obtained from satellite images while the required weather data were acquired from weather stations. The MODIS products that were used in ALARMD to calculate ETa were: Land Surface Temperature (LST) from the Daily L3 Global 1 km Grid product (MOD11A1), the 16-day albedo product (MCD43B3) describing both directional hemispherical reflectance (black-sky albedo) at local solar noon and bihemispherical reflectance (white-sky albedo), The level-4 MODIS global Leaf Area Index (LAI) every 8 days (MOD15A2), and MODIS land cover product (MCD12Q1) derived from observations spanning a year's input of Terra and Aqua data with 17 land cover classes defined by the International Geosphere Biosphere Programme (IGBP).

Different image processing techniques and algorithms were used to prepare the data downloaded from MODIS website. Images were re-projected from Sinusoidal projection to geographic coordinates and resampled to a pixel size of 1 km. The output files were then clipped to the boundaries of the study area to reduce the size of files and to remove extraneous data. Daily weather data, on the other hand were used to calculate ETo (eq.18). MODIS land cover map was used to derive crop coefficients needed to calculate ETc.

Because of the difficulty of using the image processing modeler, images were exported from image processing software and were then imported and arranged in spreadsheets. Data of MODIS LST, passing time, view angle, LAI and Albedo along with solar radiation, air temperature, wind speed and plant height were inserted in spreadsheets. The model was applied on the data to calculate EWSI values for the corresponding data. Outputs were then exported, on the form of point data, to geographic information system (GIS) to generate maps of EWSI using bilinear interpolation method. An example will be discussed for the image of July 1st, 2009.

4.3 Initial results and future work

Output from the EWSI maps showed that the extent of drought was variable inside the study area. Within the study area, EWSI ranged from 0.56 to 0.84, which indicated that actual evapotranspiration was lower than the reference evapotranspiration. This could indicate the end of season for rainfed crops. Comparing the result from EWSI and the map of NDVI deviation, more details on drought could be obtained from the former. The trend of EWSI could be attributed to the land use/cover of the study area. For example, the high values were noticed in the middle parts of the study area, where soils were poor and land was sparsely vegetated and tended to be overgrazed by herds of sheep. The relatively lower values of EWSI observed in the remaining other parts of the study area could be attributed to three factors. The first factor was the presence of clay soils (Vertisols) in the west which resulted in more soil moisture storage that increased the ALARMD ETa. The second factor which could explain the EWSI values in the northern parts of the study area was irrigation, which was practiced in these areas. The third factor which explained EWSI was the relatively low temperatures in the southern parts of the study area which were characterized by high altitudes and lower air temperatures than the other parts.

Unlike EWSI, the NDVI maps were not able to detect patterns and spatial variation of drought in the study area (Figure 13). The NDVI map showed that most of the study area did not deviate from the 10-years mean of NDVI. The eastern parts of the study area showed higher NDVI values than the average. In terms of drought, the NDVI map was less-informative when compared with EWSI. This could be attributed to the fact that NDVI values were neither correlated with land use nor with vegetation parameters. Also, the range of NDVI deviation above which drought would occur was not identified. The EWSI, on the other hand, considered the most important vegetation parameters (LAI, crop type and Kc) in drought monitoring. These initial results could indicate the usefulness of ALARMD in modeling ETa and in mapping EWSI. Future work, however, is still needed to correlate EWSI to the severity and temporal distribution of drought. Also, the use of high spatial resolution data to improve ETc estimation and EWSI maps shall be investigated.

5. Acknowledgement
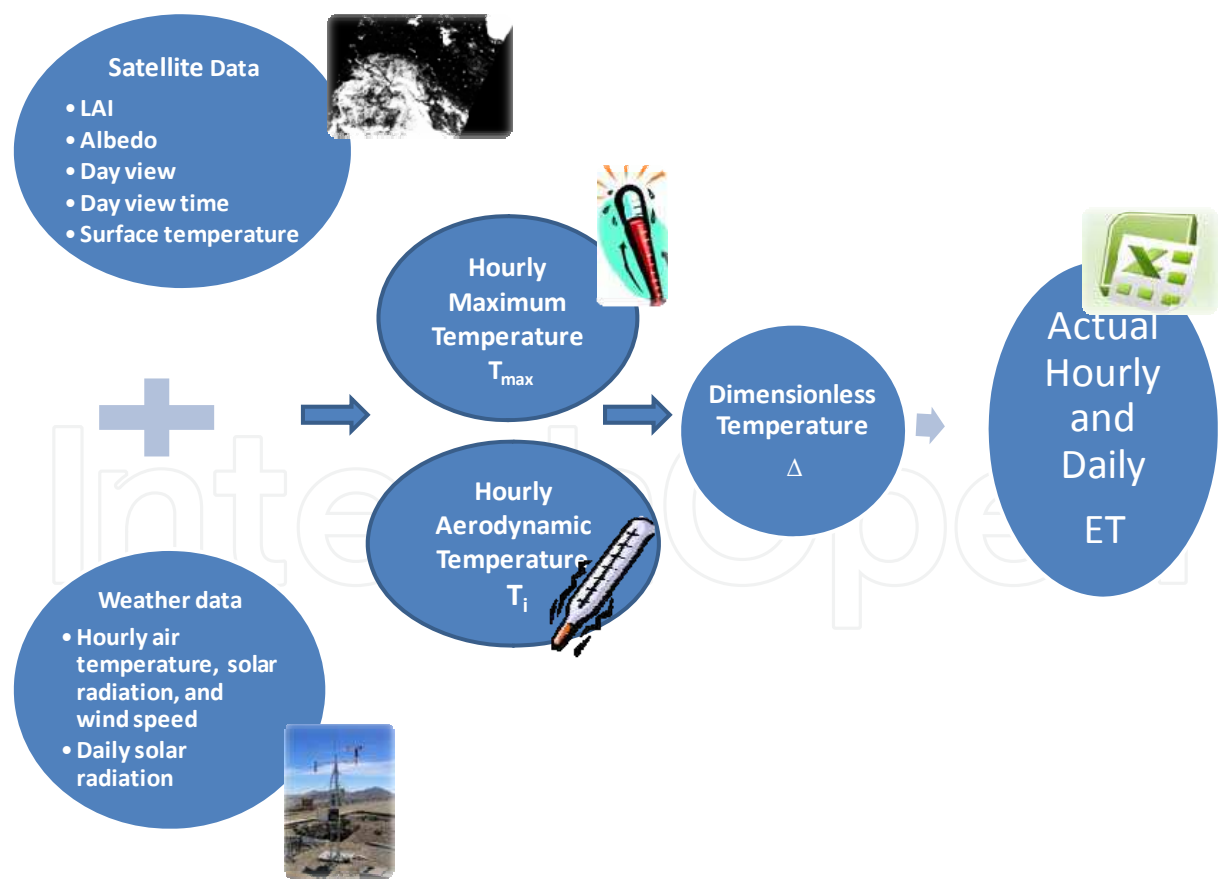
Fig. 1. ALARM and dimensionless temperature (ALARMD) calculations of actual hourly and daily evapotranspiration.
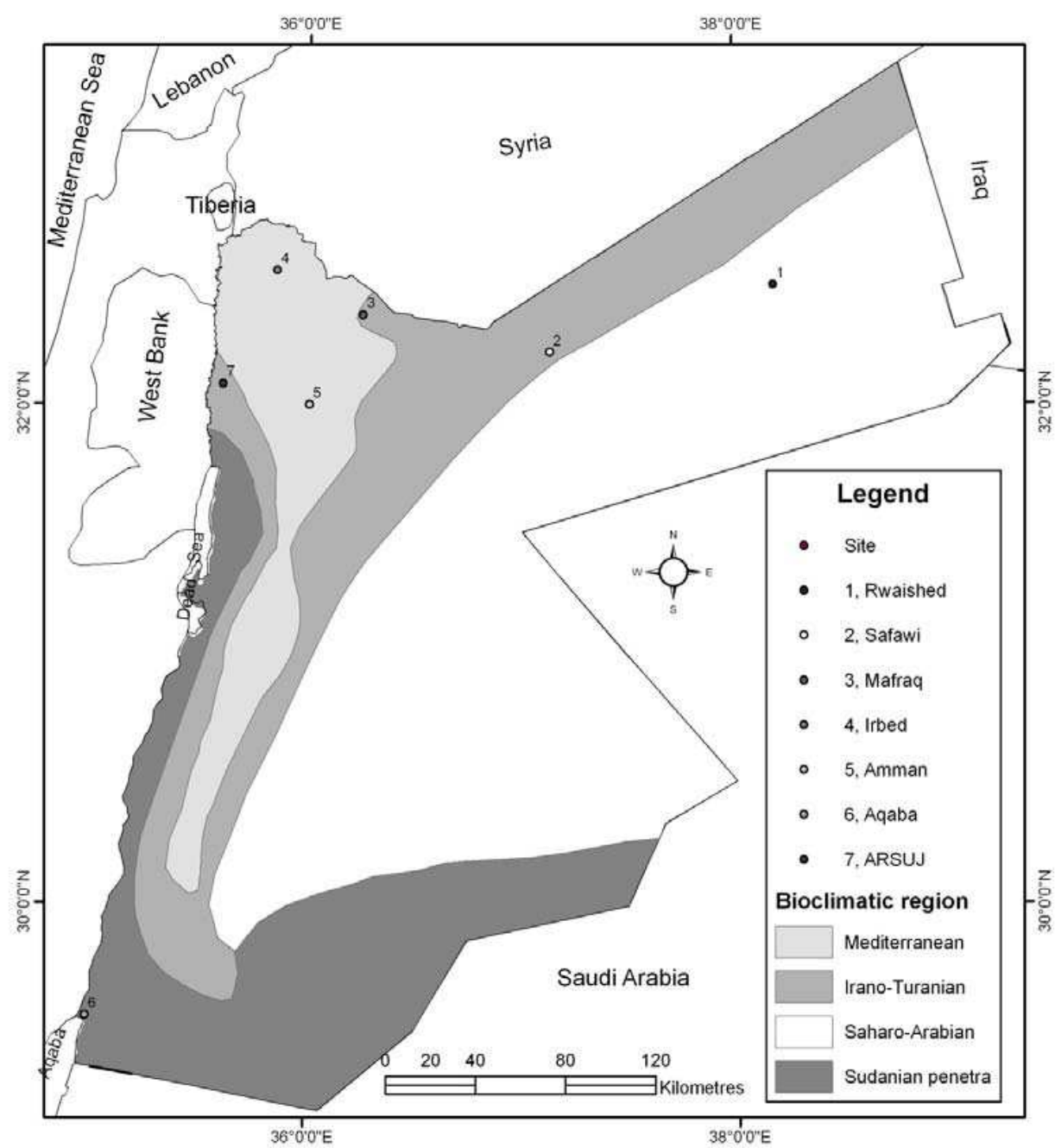
Fig. 2. Locations of the validation and comparison sites in Jordan.
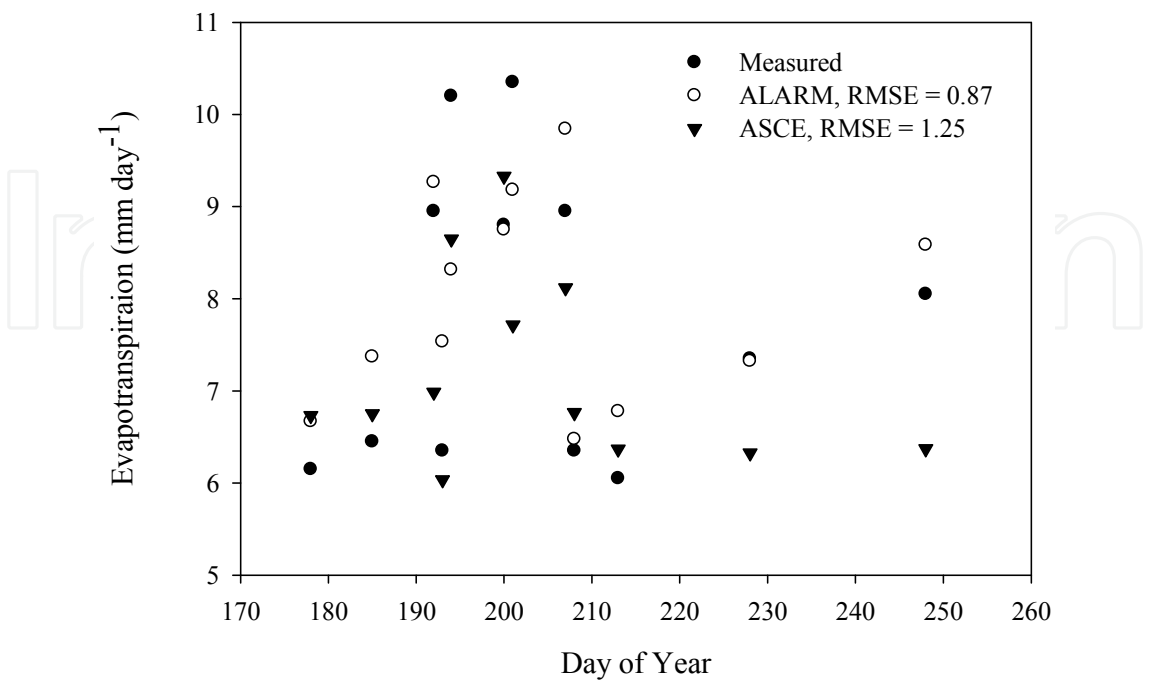
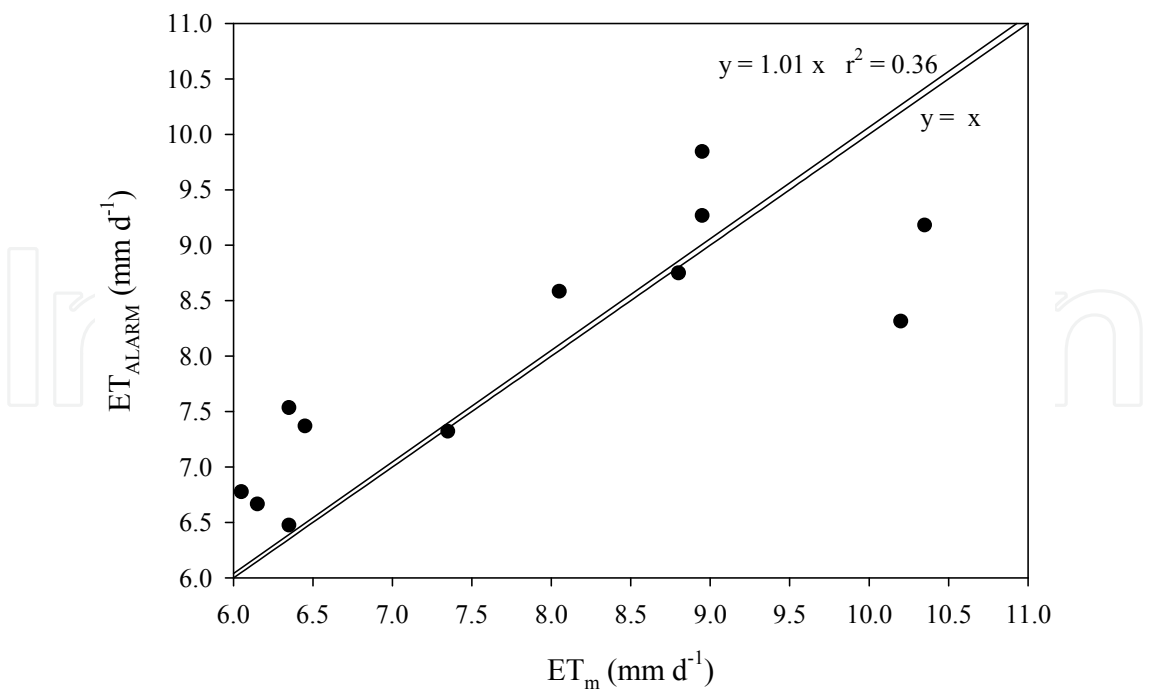Fig. 3. Measured, ALARMD and ASCE evapotranspiration at the validation site.

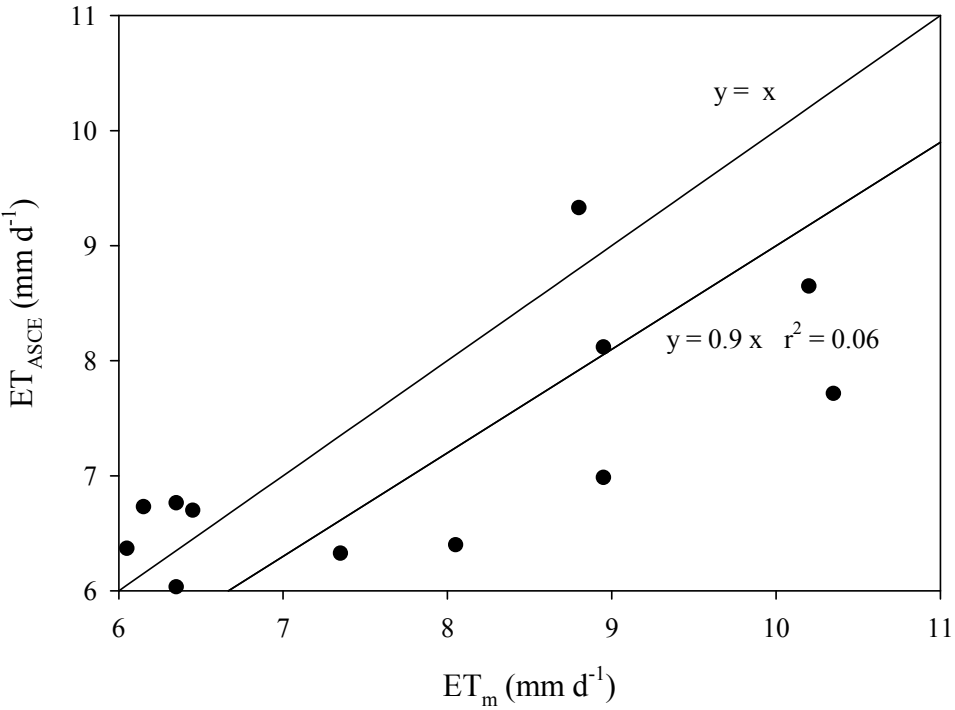Fig. 4. ALARMD vs. measured evapotranspiration at the validation site

Fig. 5. ASCE vs. measured evapotranspiration at the validation site
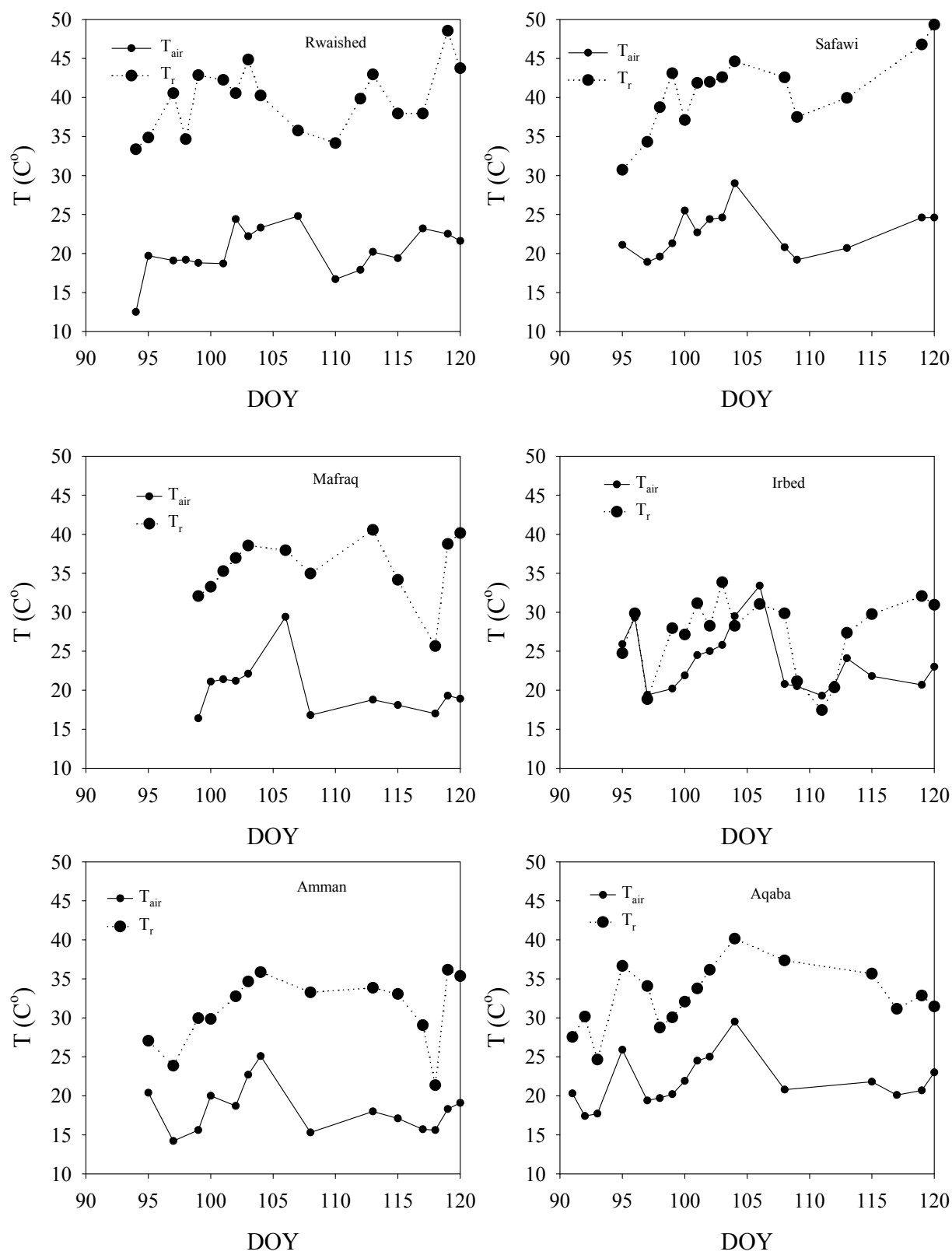
Fig. 6. Air (T_{air}) and radiometric surface temperature (T_r) on different days of year (DOY) during April 2005 for the six sites.
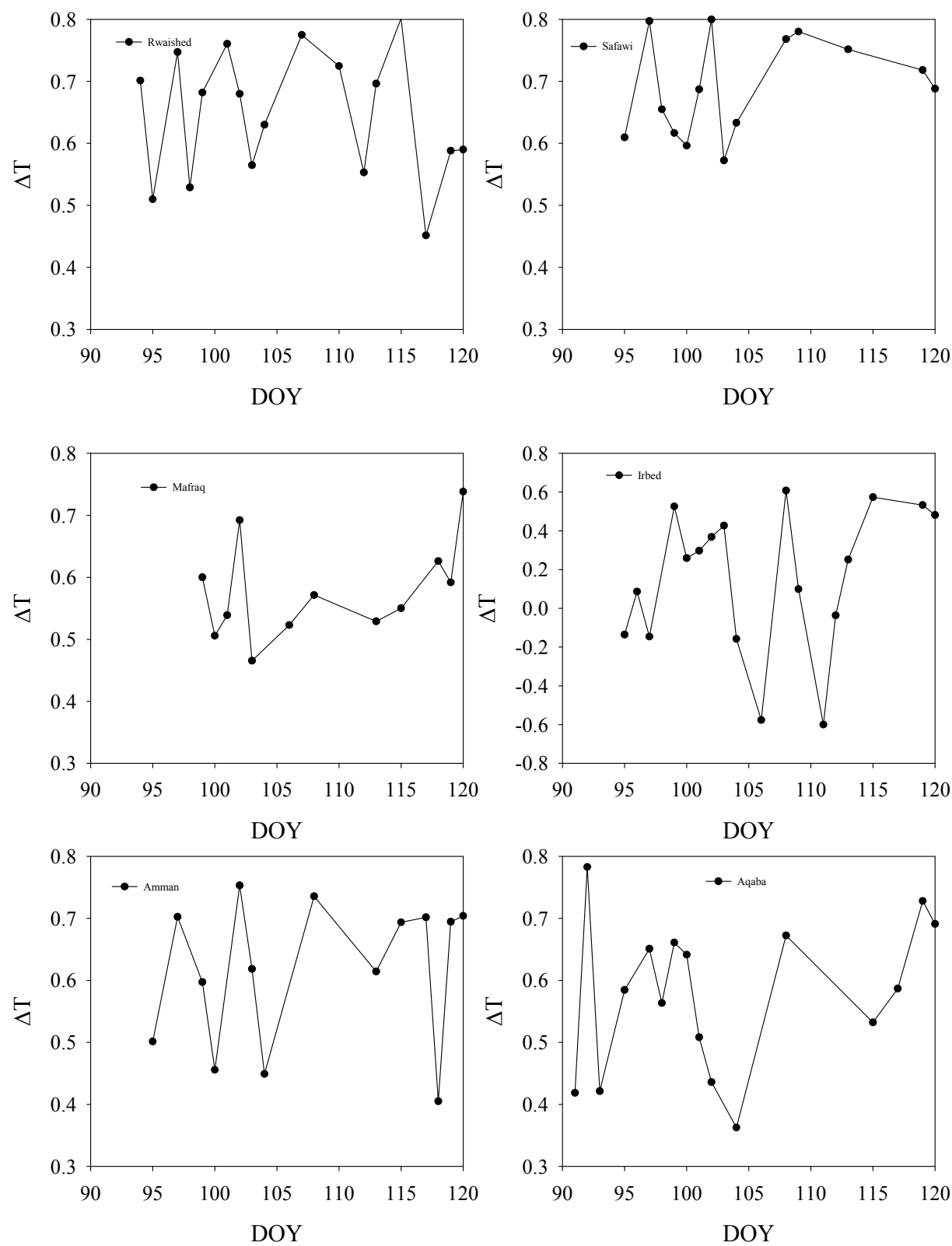
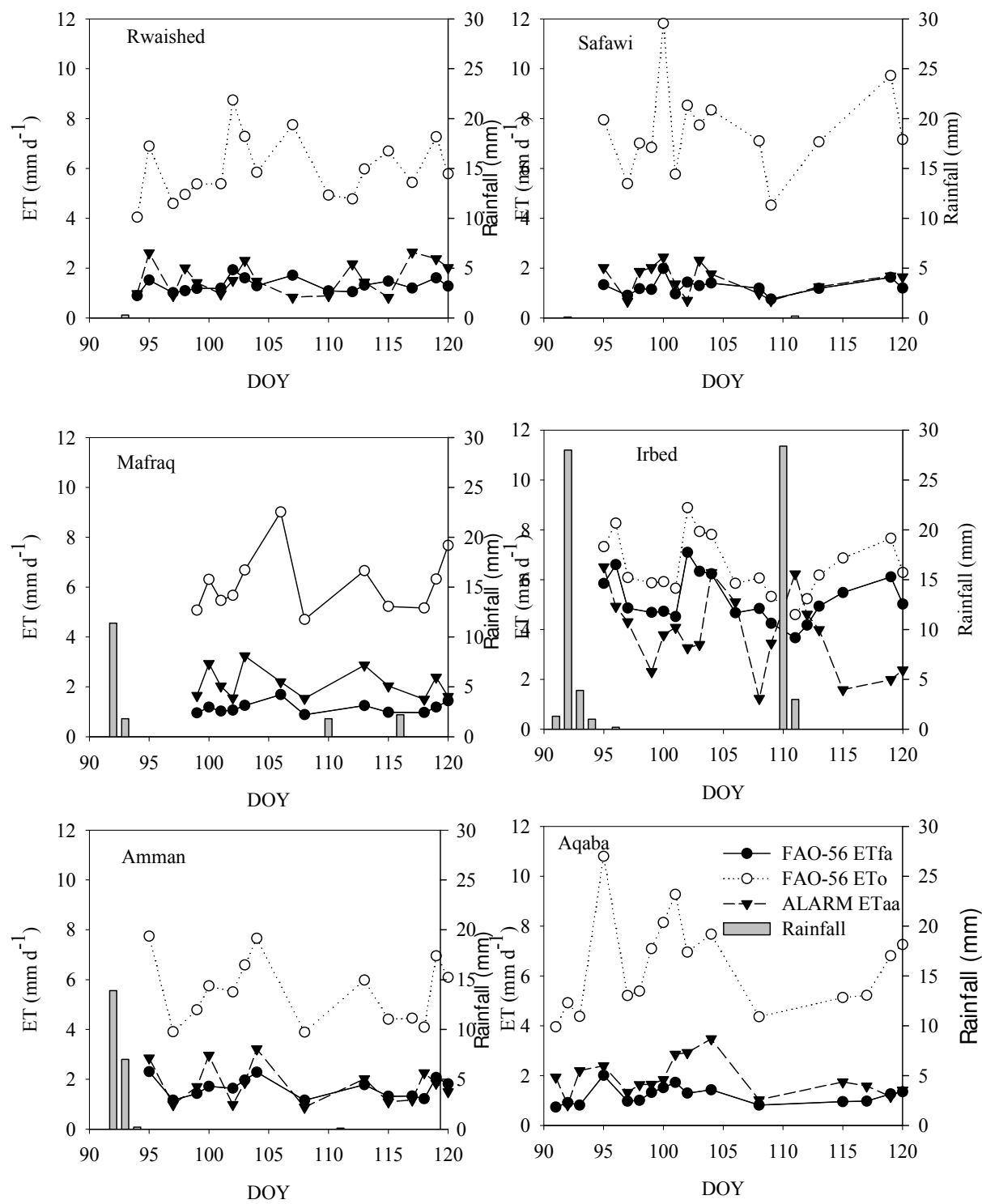Fig. 7. Dimensionless temperature (Δ_T) on different days of year (DOY) during April 2005 for the six sites.

Fig. 8. Daily actual ALARMD (ET_{aa}), FAO-56 (ET_{fa}) and FAO-56 grass reference (ET_o) evapotranspiration and daily rainfall amounts on different days of year (DOY) April 2005 for the six sites.
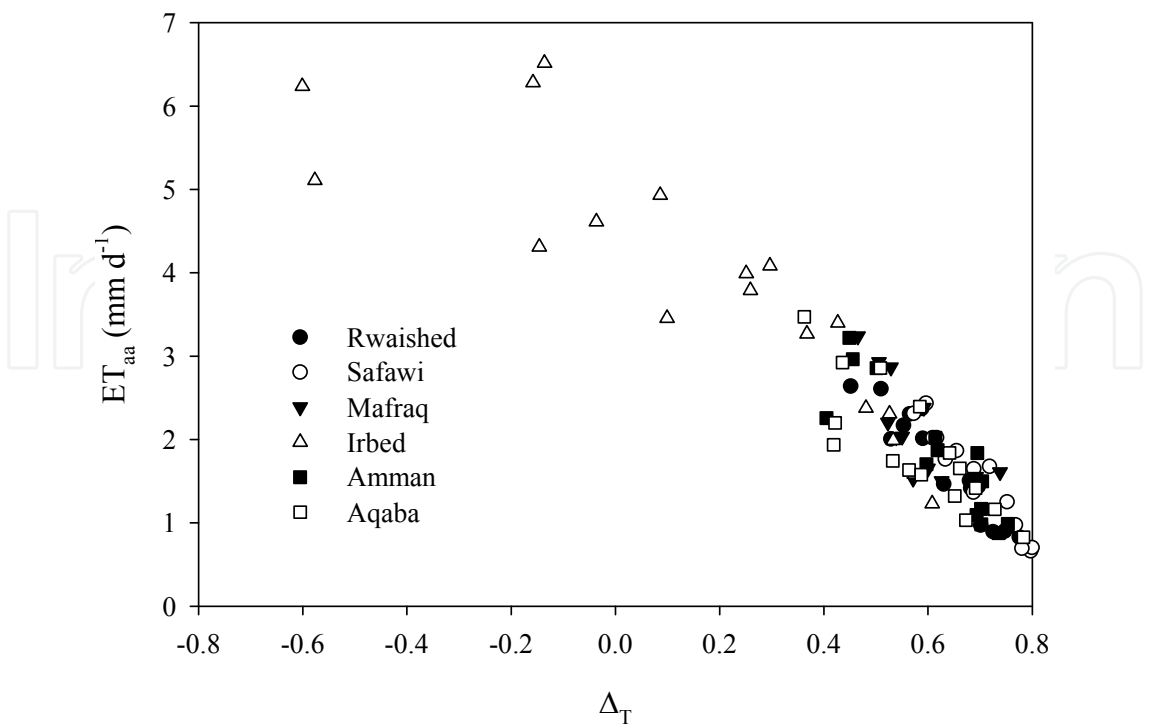
Fig. 9. Relationship between the ALARMD daily actual evapotranspiration (ET_{aa}) and the dimensionless temperature (Δ_T).
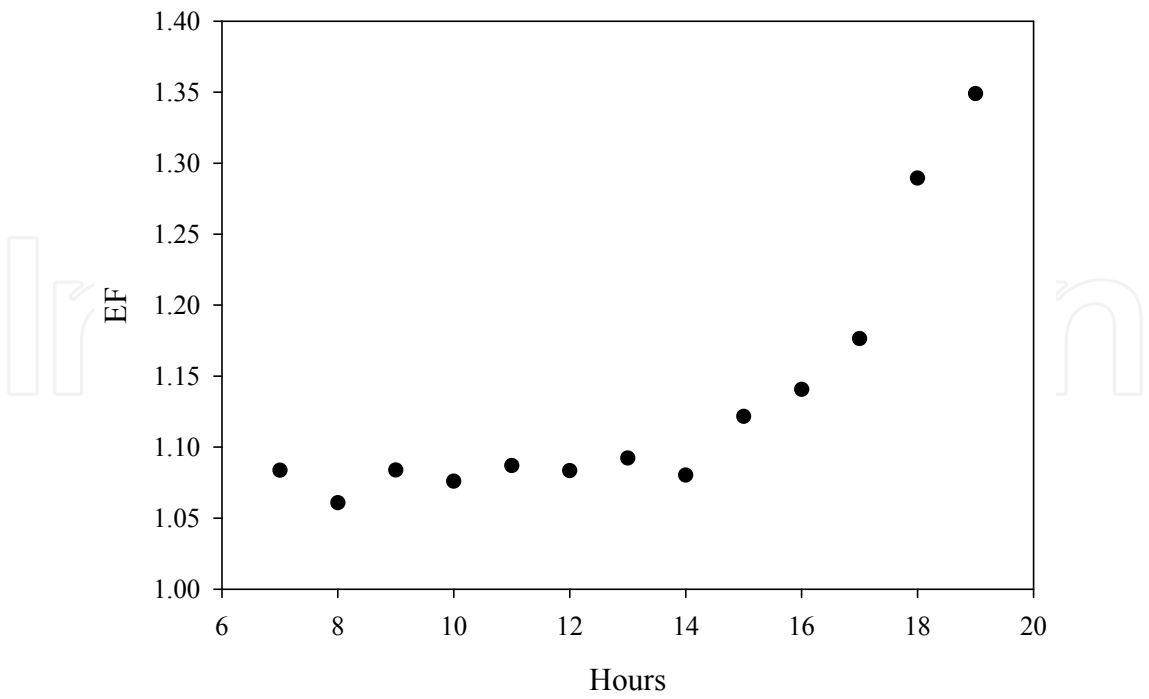

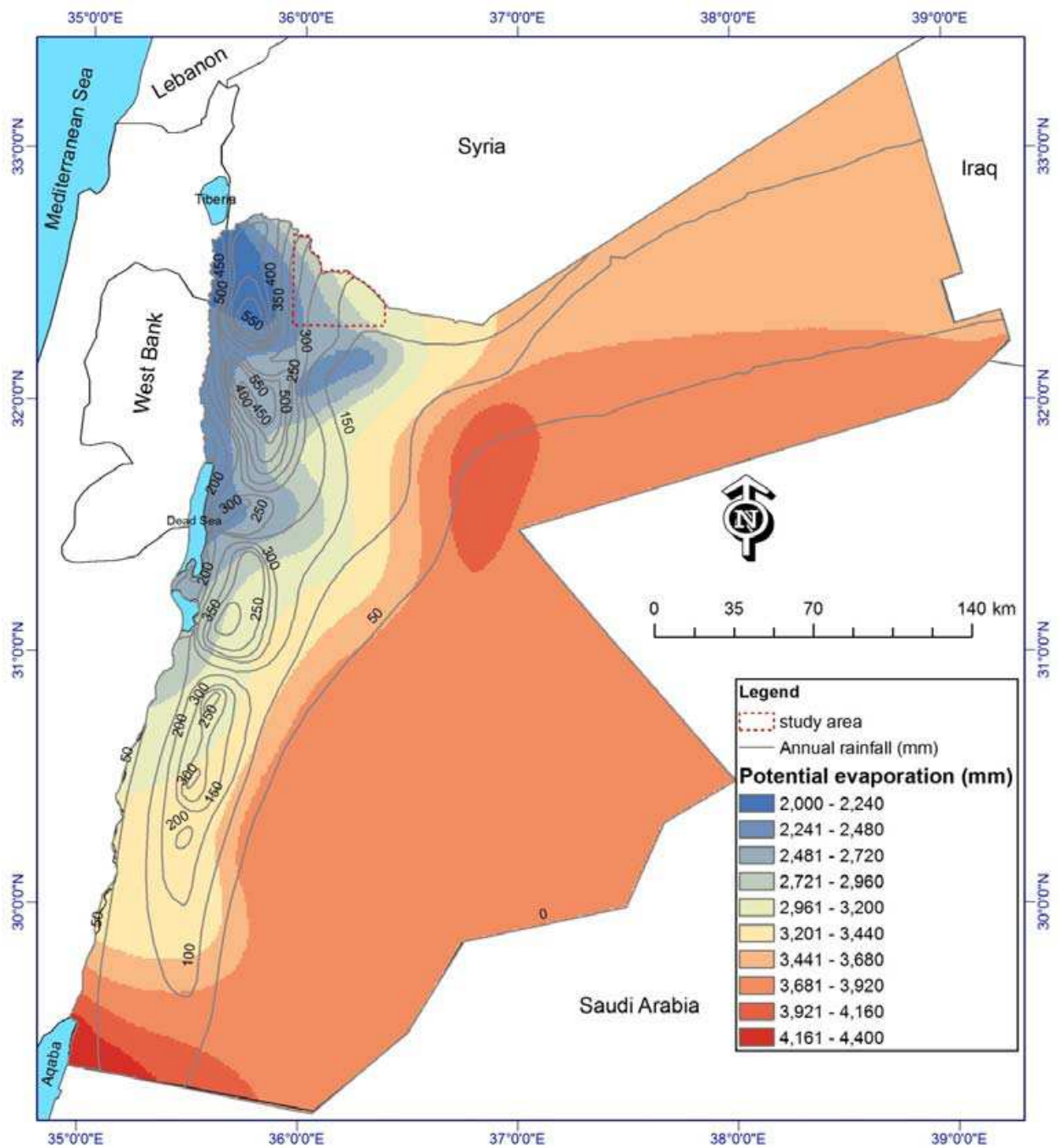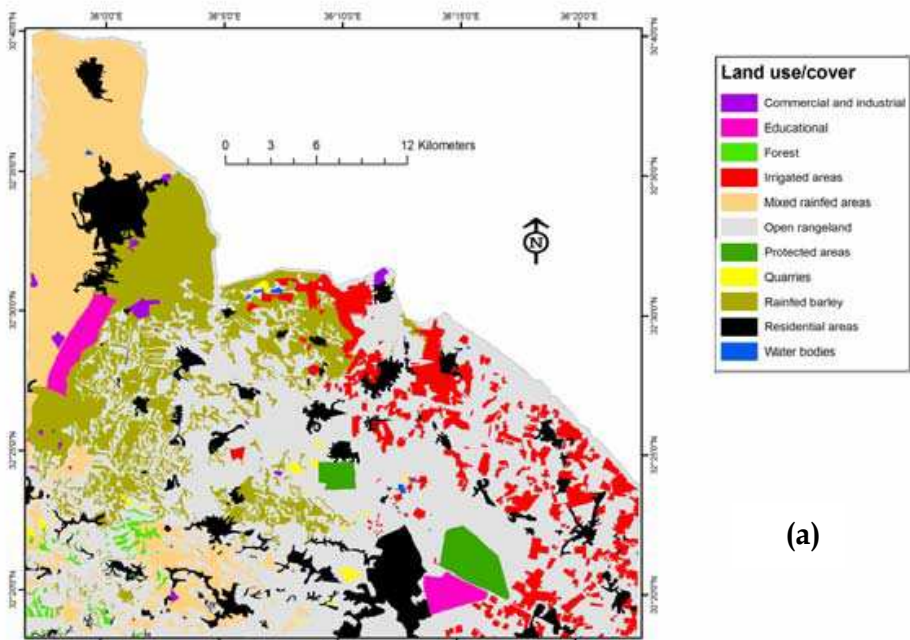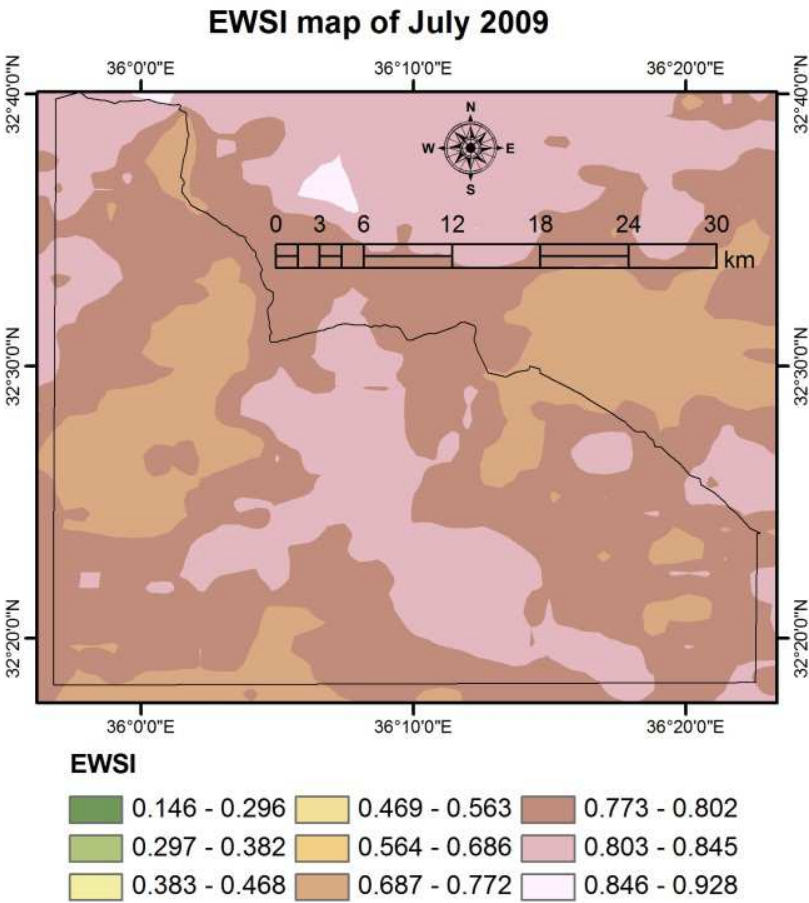Fig. 10. Hourly evaporative fraction (EF) on July 5th, 2009 in Blythe, California.

Fig. 11. Mean annual rainfall and potential evaporation in Jordan (1971-2005).

(a)

EWSI map of July 2009

EWSI

0.146 - 0.296	0.469 - 0.563	0.773 - 0.802
0.297 - 0.382	0.564 - 0.686	0.803 - 0.845
0.383 - 0.468	0.687 - 0.772	0.846 - 0.928

(b)

NDVI deviation 25 June- 10 July

NDVI deviation
- -0.2 to -0.4
- -0.1 to -0.2
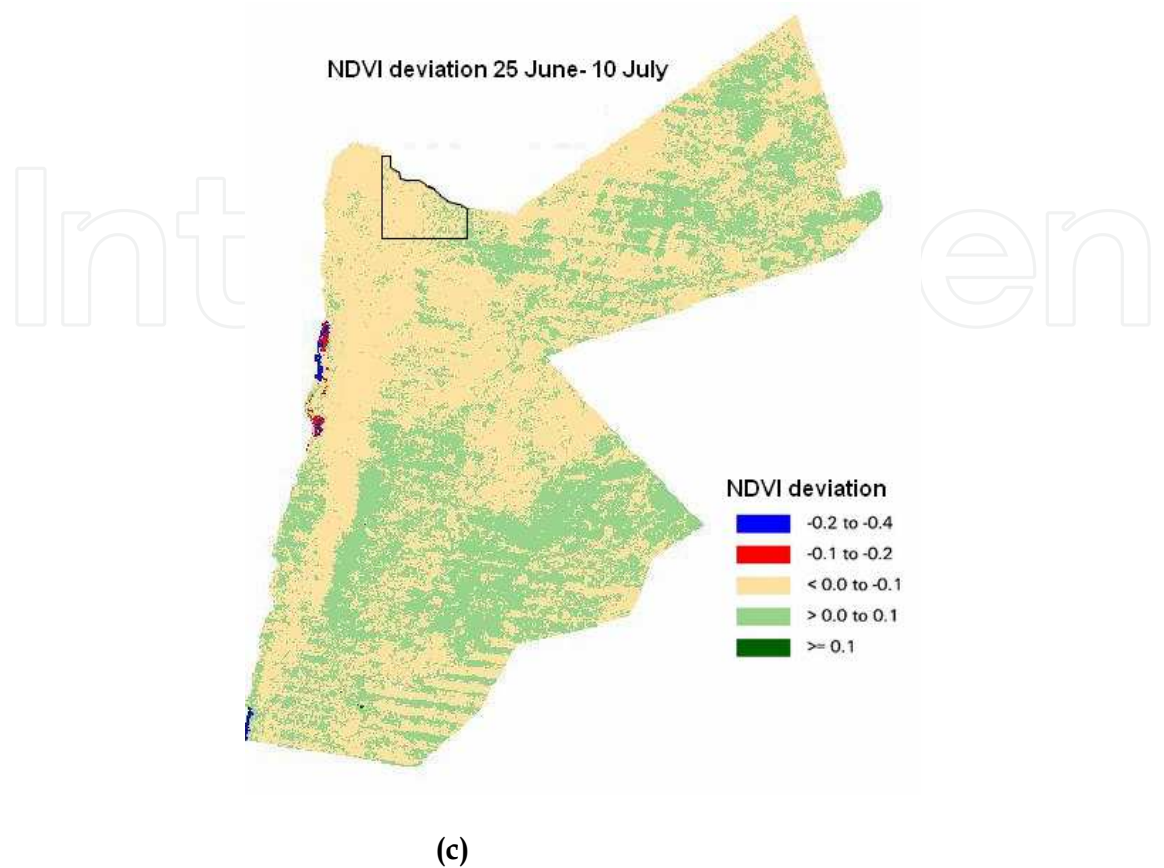- < 0.0 to -0.1
- > 0.0 to 0.1
- >= 0.1

(c)

Fig. 12. Maps of land use/cover map of Yarmouk basin study area (a), EWSI of 1 July (b), and NDVI deviation map for the period 25 June-10 July for Jordan and the study area (c).

	Oct.-Nov. 2001	Dec. 2001	Jan. 2002	Feb. 2002	Mar. 2002	Apr. 2002	Total	% of Annual Average*
				(mm)				
Rwaished	32.1	16.2	28	5.9	3.2	0.3	85.7	106
Safawi	28.9	17.6	37.7	12.8	5.7	0.3	103	138
Mafraq	19	65.2	81.4	13.9	39	17.2	235.7	149
Irbed	51.2	205.1	133.3	40.4	117.7	65.8	617.5	136
Amman	20.3	93.8	109.8	29.3	38.4	21.2	314.2	115
Aqaba	9.3	1	3	4.4	0	0	17.7	58

*: Based on annual average from 1922/1923-1999/2000 (Jordan Meteorological Department, http://www.jmd.gov.jo)

Table 1. Monthly precipitation for the comparison study sites in Jordan (mm) in the 2001/2002 season.

	Continuous urban	Green urban	Rainfed crops	Irrigated olives	Rangeland*	Bare rock	Weighted K_sK_c
Rwaished	38.0	9.5	--	5.5	47.0	--	0.22
Safawi	29.6	7.4	--	1.7	51.1	10.2	0.17
Mafraq	3.6	0.9	--	--	95.5	--	0.19
Irbed	20.2	5.0	67.8	7.0	--	--	0.80
Amman	57.5	6.4	--	21.2	14.9	--	0.30
Aqaba	32.9	16.1	--	--	51.0	--	0.19
K_sK_c	0.00	1.00	1.00	1.00	0.15	0.00	

* Mafraq site includes 70.3 % of protected rangeland K_sK_c = 0.20) while Aqaba includes bare sandy soils with a very sparse vegetation (K_sK_c = 0.05).

Table 2. Land use/cover percent, water stress and crop coefficient (K_sK_c) and the weighted K_sK_c for each site.

Station	LAI	T_r	T_r Availability	T_r Availability
	(m² m⁻²)	(C°)	(d)	(%)
Rwaished	0.10-0.40	33.4-48.6	18	60
Safawi	0.20-0.50	30.7-49.3	14	47
Mafraq	1.10-1.70	25.7-40.6	13	43
Irbed	0.85-0.98	17.5-33.9	18	60
Amman	0.71-1.10	21.4-36.2	15	50
Aqaba	0.20	24.6-40.2	23	77

Table 3. Leaf area index (LAI), MODIS radiometric surface temperature (T_r) and number of days for which MODIS T_r was available in April for the six sites.

	ET_{aa}			ET_{fa}			ΔT		
Stations	Min	**Max**	Ave	Min	**Max**	Ave	Min	**Max**	Ave
				(mm d⁻¹)					
Rwaished	0.8	2.6	1.6	0.9	1.9	1.3	0.45	0.80	0.65
Safawi	0.7	2.4	1.5	0.8	2.0	1.3	0.52	0.80	0.65
Mafraq	1.5	3.2	2.1	0.9	1.7	1.6	0.47	0.74	0.58
Irbed	1.2	6.5	3.9	3.7	7.1	5.2	-0.6	0.61	0.16
Amman	0.9	3.2	1.8	1.2	2.3	1.7	0.40	0.75	0.62
Aqaba	0.8	3.5	1.9	0.7	2.0	1.2	0.36	0.78	0.58

Table 4. Minimum, maximum, and average FAO-56 (ET_{fa}) and ALARM (ET_{aa}) actual evapotranspiration and dimensionless temperature (ΔT) for the six sites.

| | ET$_c$ | | | Relative Error | |
	ALARMD	SEBAL	Surface Renewal	ALARMD	SEBAL
	mm hr^{-1}			(%)	
Pixel 1	0.93	0.77	0.87	6.9	-11.5
Pixel 2	0.86	0.75	0.87	-1.1	-13.8
Pixel 3	1.0	0.8	0.87	14.9	-8.0
Pixel 4*	1.0	0.8	0.87	14.9	-8.0
Average	**0.94**	**0.78**	**0.87**	**8.0**	**-10.3**

*: The surface renewal station was located at Pixel 4.

Table 5. ALARMD and SEBAL ASTER 90-m pixel hourly Evapotranspiration.

| | ET$_c$ | | | Relative Error | |
	ALARMD	SEBAL	Surface Renewal	ALARMD	SEBAL
	mm day^{-1}			(%)	
Pixel 1	8.5	7.1	8.6	-1.2	-17.4
Pixel 2	7.9	6.9	8.6	-8.1	-19.8
Pixel 3	9.2	7.4	8.6	7.0	-14.0
Pixel 4	9.2	7.4	8.6	7.0	-14.0
Average	**8.7**	**7.2**	**8.6**	**1.2**	**-16.3**

Table 6. ALARMD and SEBAL ASTER 90-m pixel daily Evapotranspiration.

	ALARMD	SEBAL
	ET$_c$ (mm day^{-1})	
Pixel 1	6.6	6.4
Pixel 2	7.6	6.7
Pixel 3	6.3	6.1
Pixel 4	7.4	6.6
Pixel 5	6.6	6.1
Pixel 6	7.6	6.5
Pixel 7	7.4	6.4
Pixel 8	7.6	6.4
Average	**7.1**	**6.4**

Table 7. ALARMD and SEBAL MODIS 1-km pixel daily Evapotranspiration.

	ALARM-D	SEBAL
	ET$_c$ (mm day^{-1})	
Pixel 2	8.1	6.9
Pixel 4	8.9	7.0
Pixel 6	9.0	7.0
Pixel 8	6.8	6.1
Average	**8.2**	**6.8**

Table 8. ALARM-D and SEBAL ASTER 1-km pixel daily Evapotranspiration.

6. References

Al-Bakri, J.T., Suleiman, A.A., 2004: NDVI response to rainfall in the different ecological zones in Jordan. *International J. Remote Sens.*, 25(19), 3897–3912.

Al-Bakri J. T., Taylor J. C., 2003: Application of NOAA-AVHRR for monitoring vegetation conditions and biomass in Jordan. *Journal of Arid Environments*, 54(3): 579-593.

Al-Eisawi, D.M., 1985: Vegetation of Jordan. In: A. Hadidi, (ed.), Studies in the History and Archaeology of Jordan. Vol I. (pp. 45-57). Dept. of Antiquities, Amman Jordan.

Al-Jitan, M.A., 2005: Evapotranspiration of major crops in the Jordan Valley using remote sensing techniques compared with estimated field measurement using eddy-correlation. PhD Thesis, University of Jordan, Amman, Jordan.

Al-Naber G., Al-Bakri J. , Saba M., 2009: Monitoring drought and desertification in Jordan with remote sensing. Proceedings of the remote sensing and GIS applications symposium, 20 April, 2009, Geography Department, Faculty of Arts, University of Jordan, Amman, Jordan.

Allen, R.G., Pereira, L.A., Raes, D., Smith, M., 1998: Crop evapotranspiration. FAO Irrigation and Drainage Paper 56. FAO, Rome, Italy, 293 p.

Allen, R.G., Tasumi, M., Morse, A.T., and Trezza R., 2005: A LANDSAT-based energy balance and evapotranspiration model in Western US water rights regulation and planning. *J. Irrig. and Drain. Systems.*, 19, 251-268.

Allen, R.G., Tasumi, and Trezza R., 2007: Satellite-Based Energy Balance for Mapping Evapotranspiration with Internalized Calibration (METRIC)—Model. *J. Irrig. and Drain. Engrg.*, 133(4), 380-394.

ASCE (American Society of Civil Engineers), 2005: The ASCE Standardized Reference Evapotranspiration Equation, edited by Allen, R.G., Walter, I.A., Elliott, R., Howell, T., Itenfisu, D., and Jensen, M., ASCE-EWRI Task Committee Report, January, 2005.

Anderson, M.C., Norman, J.M., Mecikalski, J.R., Otkin, J.A., and Kustas, W.P., 2007: A climatological study of evapotranspiration and moisture stress across the continental United States based on thermal remote sensing: 1. Model formulation. *J. Geophys. Res.*, 112(D10), D11112, doi:10.1029/2006JD007507.

Bandara, K.M.P.S., 2003: Monitoring irrigation performance in Sri Lanka with high-frequency satellite measurements during the dry season. *Agric. Water Manage.* 58(2), 159-170.

Bastiaanssen, W.G.M., Chandrapala, L., 2003: Water balance variability across Sri Lanka for assessing agricultural and environmental water use. *Agric. Water Manage.*, 58(2), 171-192.

Bastiaanssen, W.G.M., Menenti, M., Fwddws, R.A., Holtslag, A.A.M., 1998: A remote sensing surface energy balance algorithm for land (SEBAL). *J. Hydrol.*, 212/213, 198-212.

Ben-Asher, J., Phene, C.J., Kinarti, A., 1992: Canopy temperature to assess daily evapotranspiration and management of high frequency drip irrigation systems. *Agric. Water Manage*. 22(4), 379-390.

Brutsaert, W., 1982: Evaporation into the Atmosphere, D. Reidel, Boston, 299 pp.

Brutsaert, W., Chen, D., 1996: Diurnal variation of surface fluxes during thorough drying (or severe drought) of natural prairie. *Water Resour. Res.*, 32(7), 2013-2019.

Brutsaert, W., and Sugita, M., 1996: Sensible heat transfer parameterization for surfaces with anisothermal dense vegetation, *J. Atmos. Sci.*, 53(2), 209-216.

Consoli, S., D'Urso, G., Toscano, A., 2006: Remote sensing to estimate ET-fluxes and the performance of an irrigation district in southern Italy. *Agric. Water Manage.* 81 (3), 295-314.

Chandrapala, L., Wimalasuriya, M., 2003: Satellite measurements supplemented with meteorological data to operationally estimate evaporation in Sri Lanka. *Agric. Water Manage.* 58(2), 89-107.

Crago, R. D., 1998: Radiometric and equivalent isothermal surface temperatures. *Water Resour. Res.*, 34(11), 3017-3023.

Crago, R.D., Brutsaert, W., 1996: Daytime evaporation and the self-preservation of the evaporative fraction and the Bowen ratio. *J. Hydro.*, 178, 241-255.

Crago, R., Suleiman, A.A., 2005: Heat flux parameterization for sparse and dense grasslands with the Analytical Land-Atmosphere Radiometer Model (ALARM). *Boundary Layer Meteorol.*, 114(3), 557-572.

Friedl, M. A., Davis, F. W., 1994: Sources of variation in radiometric surface temperature over a tallgrass prairie. *Remote Sens. Environ.*, 48, 1-17.

Gurney, R.J., Hsu, A.Y., 1990: Relating evaporative fraction to remotely sensed data at the FIFE site. *In* F.G. Hall and P.J. Sellers (ed.). Symposium on FIFE, Anaheim, California, American Meterological Society, 112-116.

Hatfield, J.L., Perrier, A., and Jackson, R.D., 1983: Estimation of evapotranspiration at one time-of-day using remotely sensed surface temperatures. *Agric. Water Manage.*, 7(1-3), 341-350.

JMD (Jordan Meterological Department), 2002: Jordan agrometeorological Bulletin. Meteorological Department, Agrometeorological Directorate, Ministry of Transport, Amman, Jordan (http://www.jmd.gov.jo/).

Kim, C.P., Entekhabi, D., 1997: Examination of two methods for estimating regional evaporation using a coupled mixed layer and land surface model. *Water Resour. Res.*, 33(9), 2109-2116.

Kustas, W.P., Schmugge, T.J., Humes, K.S., Jackson, T.J., Parry, R., Weltz, M.A., Moran, M.S., 1993: Relationships between evaporative fraction and remotely-sensed vegetation index and microwave brightness temperature for semiarid rangelands. *J. of Appl. Meteorol.*, 32(12), 1781-1790.

Kustas, W.P., Anderson, M.C., Norman, J.M., and Li, F.Q., 2007: Utility of radiometric-aerodynamic temperature relations for heat flux estimation, *Boundary-Layer Meteorol.*, 122(1), 167-187

Liu, X.Y, Lin, E., 2005: Performance of the Priestley-Taylor equation in the semiarid climate of North China. *Agric. Water Manage*, 71(1), 1-17.

Lhomme, J. P., Chegbouni, A., Monteny, B., 2000: Sensible heat flux-radiometric surface temperature relationship over sparse vegetation: Parameterizing B^{-1}. *Boundary-Layer Meteorol.*, 97, 431-457.

Lhomme, J.P., Elguero, E., 1999: Examination of evaporative fraction diurnal behavior using a soil-vegetation model coupled with a mixed-layer model. *Hydrol. and Earth Sys. Sci.*, 3(2), 259-270.

Loheide II, S.P., and Gorelick, S.M. 2005: A local-scale, high resolution evapotranspiration mapping algorithm (ETMA) with hydrological applications at riparian meadow restoration sites. *Remote Sens. of Environ.*, 98, 182-200.

Mahrt, L., and Vickers, D. 2004: Bulk formulation of the surface heat flux. *Boundary-Layer Meteorol.*, 110, 357-379.

Massman, W. J., 1999: A model study of kB_H^{-1} for vegetated surfaces using 'localized near-field Lagrangian theory. *J. Hydrol.*, 223, 27-43.

Menenti, M., Choudhury, B.J., 1993: Parameterization of land surface evavotranspiration using a location dependent potential evapotranspiration and surface temperature range. In Exchange processes at the land surface for a range of space and time series, Bolle H.J., R.A. Feddes, and J.D. Kalma (Eds). *IAHS Publ*, 212, 561-568.

MoA (Ministry of Agriculture, Jordan), 1994: The Soils of Jordan: Semi-detailed Level (1:50 000). National Soil Map and Land Use Project, Ministry of Agriculture, Amman, Jordan (Maps available at http://alic.arid.arizona.edu/jordansoils/_html/about.html).

MoE (Ministry of Environment, Jordan), 2006: National Action Plan and Strategy to Combat Desertification. Amman, Jordan: Ministry of Environment (Document available at http://www.unccd.int/).

Nagler, P. L. , Cleverlyb, J., Glenna, E., Lampkinc, D., Huete, A., Wan, Z., 2005: Predicting riparian evapotranspiration from MODIS vegetation indices and meteorological data. *Remote Sens. of Environ.*, 94, 17-30.

NCARE, National Center for Agricultural Research and Extension. 2002a: Annual report of Rainfed Program: Maru Agricultural Station, Irbed. NCARE, Baqa'a, Jordan (Hardcopy can be supplied by authors).

NCARE, National Center for Agricultural Research and Extension. 2002b: Irrigation Management Information System (IMIS) (Data available under IMIS-NCARTT, http://www.ncare.gov.jo/).

Qiu, G.Y., Shi, P., and Wang, L., 2006: Theoretical analysis of a remotely measurable soil evaporation transfer coefficient. *Remote Sens. of Environ.*, 101, 390-398.

Qualls, R.J., Yates, D. N., 2001: Directional radiometric temperature profiles in a grass canopy. *Advances in Water Resour. Res.*, 24, 145-155.

Roerrink, G.L., Su, Z., Menenti, M., (2000). S-SEBI A simple remote sensing algorithm to estimate the surface energy balance. *Phys. Chim. Earth (B)*, 25(2), 147-157.

Rosenberg, N.J., Verma, S.B., 1978: Extreme Evapotranspiration by Irrigated Alfalfa: A Consequence of the 1976 Midwestern Drought. *J. Applied Meteorol.*, 17, 934-941.

Santanello Jr., J.A., Friedl M.A., 2003: Diurnal covariation in soil heat flux and net radiation. *J. Appl. Meteorol.*, 42, 851-862.

Senay, G.B., Budde, M., Verdin, J.P.), Melesse, A.M., 2007: A coupled remote sensing and simplified surface energy balance approach to estimate actual evapotranspiration from irrigated fields. *SENSORS*, 7(6), 979-1000.

Shuttleworth, W.J., Gurney, R.J., Hsu, A.Y., Ormsby, J.P., 1989: FIFE: The variation in energy partition at surface flux sites. *IAHS Publ.*, 186, 67-74.

Strahler, A.H., Muller, J.P. and MODIS Science Team Members, 1999: MODIS BRDF/Albedo Product: Algorithm Theoretical Basis Document. MODIS Version 5 Land Data Products (available at: http://modis.gsfc.nasa.gov/)

Stull, R.B., 1988: An Introduction to Boundary Layer Meteorology, Kluwer Academic, 666 pp.

Suleiman, A. A., Crago R.D., 2002a: Analytical land atmosphere radiometer model (ALARM) applied to a dense canopy. *Agric. Forest Meteorol.*, 112, 151-159.

Suleiman, A. A., Crago R.D., 2002b: Analytical land atmosphere radiometer model. *J. Appl. Meteorol.*, 41, 177-187.

Suleiman, A.A., Crago, R.D., 2004: Hourly and daytime evapotranspiration using radiometric surface temperatures. *Agronomy J.*, 96, 384-390.

Suleiman, A.A., Ritchie, J.T., 2003: Modeling soil water redistribution under second stage evaporation. *Soil Sci. Soc. Am. J.*, 67(2), 377-386.

Suleiman, A.A., Ritchie, J.T., 2004: Modifications to the DSSAT vertical drainage model for more accurate soil water dynamics estimation. *Soil Sci.*, 169(11), 745-757.

Tasumi, M., R. Trezza , R.G. Allen and J. L. Wright. 2005: Operational aspects of satellite-based energy balance models for irrigated crops in the semi-arid U.S *J. Irrig. and Drain. Systems.* 19, 355-376.

Venturini, V., Gautam Bisht, G., Islam, S., Jiang, L., 2004: Comparison of evaporative fractions estimated from AVHRR and MODIS sensors over South Florida. *Remote Sens. of Environ.*, 93, 77-86.

Wald, L., Albuisson, M., Best, C., Delamare, C., Dumortier, D., Gaboardi, E., Hammer, A., Heinemann, D., Kift, R., Kunz, S., Lefèvre, M., Leroy, S., Martinoli, M., Ménard, L., Page, J., Prager, T., Ratto, C., Reise, C., Remund, J., Rimoczi-Paal, A., Van der Goot, E., Vanroy, F., and Webb, A., 2002: SoDa: a project for the integration and exploitation of networked solar radiation databases. *In*: Environmental Communication in the Information Society, W. Pillmann, K. Tochtermann Eds, Part 2, pp. 713-720. Published by the International Society for Environmental Protection, Vienna, Austria.

Wan, Z., Zhang, Y., Zhang, Q., and Li, Z., 2002: Validation of the land-surface temperature products retrieved from Terra Moderate Resolution Imaging Spectroradiometer data. *Remote Sens. Environ.*, 83, 163-180.

Wang, J., Sammis, T.W., Meier, C.A., Simmons, L.J., Miller, D.R., and Samani, Z., 2005: A modified SEBAL model for spatially estimating pecan consumptive water use for Las Cruces, New Mexico. The 15th Conference on Applied Climatology/13th Symposium on Meteorological Observations and Instrumentation, Savannah, GA, June 2005.

Zhang, L., and Lemeur, R., 1995: Evaluation of daily evapotranspiration estimates from instantaneous measurements. *Agric. Forest Meteorol.*, 74, 139-154.

Zibognon, M., Crago, R.D., and Suleiman, A.A., 2002: Conversion of radiometric to aerodynamic surface temperature with an anisothermal canopy model. *Water Resour. Res.*, 38(6), 3-1 to 3-6.
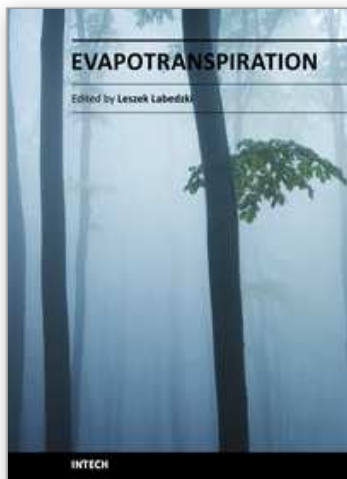
Evapotranspiration

Edited by Prof. Leszek Labedzki

Evapotranspiration is a very complex phenomenon, comprising different aspects and processes (hydrological, meteorological, physiological, soil, plant and others). Farmers, agriculture advisers, extension services, hydrologists, agrometeorologists, water management specialists and many others are facing the problem of evapotranspiration. This book is dedicated to further understanding of the evapotranspiration problems, presenting a broad body of experience, by reporting different views of the authors and the results of their studies. It covers aspects from understandings and concepts of evapotranspiration, through methodology of calculating and measuring, to applications in different fields, in which evapotranspiration is an important factor. The book will be of benefit to scientists, engineers and managers involved in problems related to meteorology, climatology, hydrology, geography, agronomy and agricultural water management. We hope they will find useful material in this collection of papers.

How to reference

In order to correctly reference this scholarly work, feel free to copy and paste the following:

INTECH
open science | open minds